minerals

MDPI

Article

Isotope Geochemistry of the Heihaibei Gold Deposit within the Kunlun River Area in the Eastern Kunlun Orogen in Northwest China and Its Metallogenic Implications

Hai-Feng Lu [1], Tong Pan [2], He Jiao [1], Qing-Feng Ding [3,*], Xuan Zhou [3] and Rui-Zhe Wu [3]

[1] Qinghai Provincial Key Laboratory of Salt Lake Resources Exploration and Research in Qaidam Basin, Qaidam Integrated Geological Exploration Institute of Qinghai Province, Golmud 816099, China
[2] Bureau of Geological Exploration and Development of Qinghai Province, Xining 810008, China
[3] College of Earth Science, Jilin University, Changchun 130061, China
* Correspondence: dingqf@jlu.edu.cn

Abstract: The Heihaibei gold deposit is located in the Eastern Kunlun Orogen in Northwest China. The gold mineralization here occurs predominantly in quartz veins within faulted granite zones. The sulfide mineral assemblage is dominated by pyrite and arsenopyrite, with minor chalcopyrite, galena, sphalerite, tetrahedrite, and micro-native gold. Weak alterations in Heihaibei granites include silicification and sericitization, with minor chloritization and carbonatization. The measured δD_{H2O} and $\delta^{18}O_{quartz}$ values of quartz in auriferous quartz veins range from −104.2‰ to −81.1‰ and +9.2‰ to +13.9‰, respectively. The $\delta^{34}S$ values of sulfides in auriferous quartz veins range from +7.60‰ to +8.65‰, and the lead isotope compositions of sulfides in ores range from 18.7219 to 19.0007 for $^{206}Pb/^{204}Pb$, 15.6959 to 15.7062 for $^{207}Pb/^{204}Pb$, and 37.7359 to 38.8055 for $^{208}Pb/^{204}Pb$. The Pb isotope compositions of potassic feldspars from Heihaibei granites vary from 18.3532 to 19.4864 for $^{206}Pb/^{204}Pb$, 15.6475 to 15.6812 for $^{207}Pb/^{204}Pb$, and 37.1750 to 38.4598 for $^{208}Pb/^{204}Pb$. Collectively, the isotope (H, O, S, and Pb) geochemistry suggests that the ore-forming fluid was a special metamorphic water evolved from the deep slab-derived fluids, and the sulfur and lead were predominantly sourced from such metamorphic fluids, and from the deep parts of the Heihaibei granites. Therefore, the Heihaibei gold deposit can be classified as an orogenic gold deposit, which is closely associated with the subduction of the Paleo-Tethys oceanic plate, and even the final closure of this ocean by the Later Triassic.

Keywords: slab-derived metamorphic water; orogenic gold deposit; Kunlun River gold field

check for updates

Citation: Lu, H.-F.; Pan, T.; Jiao, H.; Ding, Q.-F.; Zhou, X.; Wu, R.-Z. Isotope Geochemistry of the Heihaibei Gold Deposit within the Kunlun River Area in the Eastern Kunlun Orogen in Northwest China and Its Metallogenic Implications. *Minerals* **2023**, *13*, 274. https://doi.org/10.3390/min13020274

Academic Editor: Dominique Gasquet

Received: 23 December 2022
Revised: 9 February 2023
Accepted: 13 February 2023
Published: 15 February 2023

Copyright: © 2023 by the authors. Licensee MDPI, Basel, Switzerland. This article is an open access article distributed under the terms and conditions of the Creative Commons Attribution (CC BY) license (https://creativecommons.org/licenses/by/4.0/).

1. Introduction

The Eastern Kunlun Orogen (EKO) extends from east to west for more than 1200 km, with a width of 50–200 km along the northern margin of the Qinghai–Tibetan Plateau, and records the earliest amalgamation history of the Qinghai–Tibetan Plateau (Figure 1) [1,2]. The EKO, which is bounded by the Qaidam block (QDM) on the north and the Bayan Har–Songpanganzi Terrane (BH–SG) on the south, is usually considered to be composed of three sub-parallel tectonic belts from north to south, the North Kunlun belt (NKL), the Middle Kunlun belt (MKL), and the South Kunlun belt (SKL), separated by the North Kunlun fault (N. KLF), the Middle Kunlun fault (M. KLF), and the South Kunlun–Aryan Maqin fault (S. KLF–AMF), respectively [3]. Since 1999, numerous ore prospecting projects within the EKO have been deployed by the China Geology Survey [4]. So far, the EKO has become an important ore belt in which ca. 140 mineral occurrences regarding Au, Fe, Cu, Pb, Zn, W, Mo, Ni, Co, and Sb were discovered, and ca. 26 of them have become different sizes of mineral deposits in the EKO and the adjacent BH–SG (Figure 1b) [5,6]. Especially, the EKO hosts numerous gold deposits, as best represented by those in the Wulonggou gold field [4,7–13], Gouli gold field [14–19], and Kaihuangbei gold field [14,20].

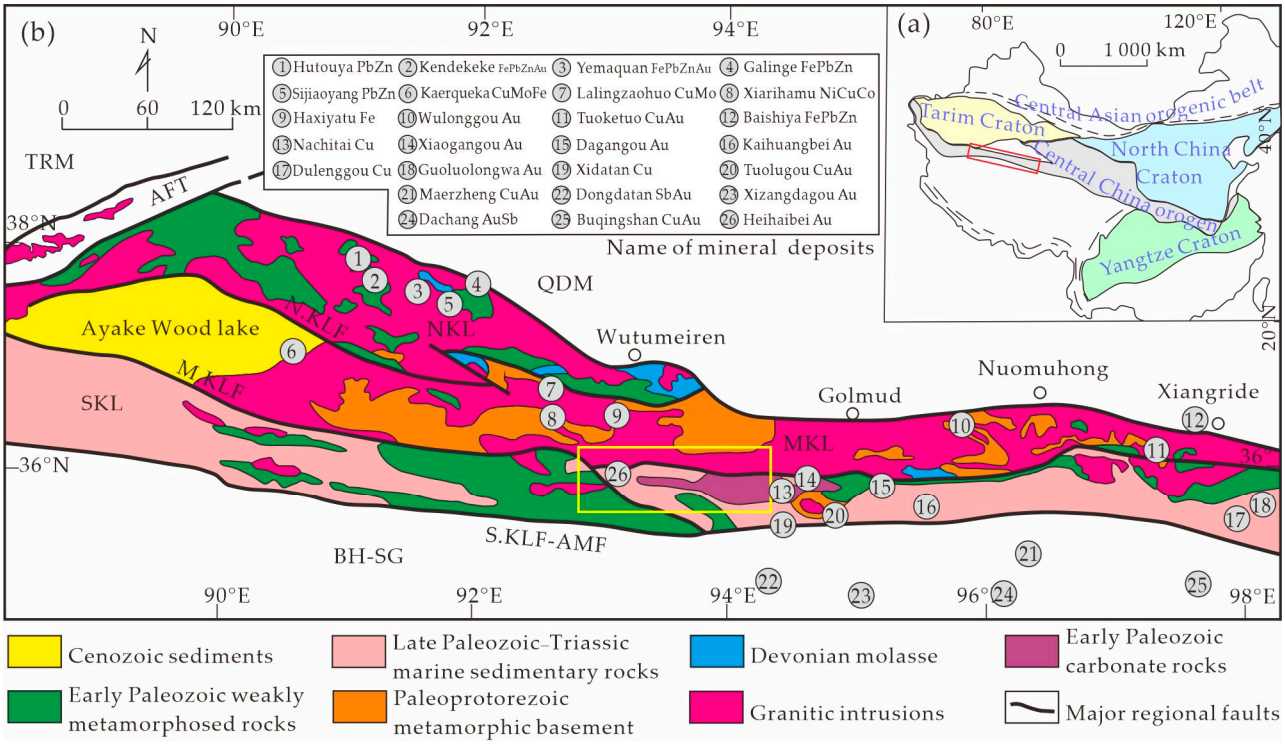


Figure 1. (**a**) Sketch map of China showing the tectonic location of the EKO, revised after [21]; (**b**) schematic geological map of the EKO, simplified and modified after [2]. EKO: Eastern Kunlun Orogen; QDM: Qaidam Block; TRM: Tarim Basin; NKL: North Kunlun Belt; MKL: Middle Kunlun Belt; SKL: South Kunlun Belt; BH–SG: Bayan Har–Songpanganzi Terrane; ATF: Altyn Tagh fault; N.KLF: North Kunlun Fault (South Qiman Tagh Fault); M.KLF: Middle Kunlun Fault; S.KLF–AMF: South Kunlun–Aryan Maqin Fault. Major mineral deposits after [5,6].

In recent years, the Kunlun River goldfield (KLRA) in the SKL has gradually become an important gold mineralization belt because more than 10 gold deposits or occurrences were discovered throughout this area (Figure 2), among which the Heihaibei gold deposit is the largest [22–25]. Thus far, few geologists have carried out geological research on the Heihaibei gold deposit or on other deposits in the KLRA. Most of the published papers or reports emphasize the geological characteristics and gold prospecting potentials for the Heihaibei gold deposit [22,24–27]. Because the dominant ore types are auriferous quartz veins, it was thought that the Heihaibei gold deposit belongs to a hydrothermal-vein-type gold deposit [22], a magmatic hydrothermal gold deposit [24], or an orogenic gold deposit [25]. Based on the geological characteristics and a few stable isotope compositions, some other gold deposits in the KLRA such as the Heihainan, Heicigou, and Dazaohuo gold deposits were also considered to belong to orogenic gold deposits [28,29] or altered-rock-type gold deposits [30], and the ore-forming fluids and materials were derived predominantly from metamorphic water and wall rocks, respectively [28,29]. However, Yu et al. (2022) argued that the Heihaibei gold deposit was a granitic intrusion-related gold deposit rather than an orogenic gold deposit, and the ore-forming fluids and materials were derived from a magmatic hydrothermal source that was closely related to the Heihaibei granites, according to their three sets of H, O, S, and Pb isotope compositions [23]. In a word, the origins of the ore-forming fluids, sources of metals, and genetic types responsible for the Heihaibei gold deposit or other gold mineralization in the Kunlunhe River area remain controversial. Systematic isotope studies on the Heihaibei gold deposit have not been carried out, and especially, a controversy between the orogenic gold deposit and the granitic intrusion-related gold deposit has persisted for a long time.

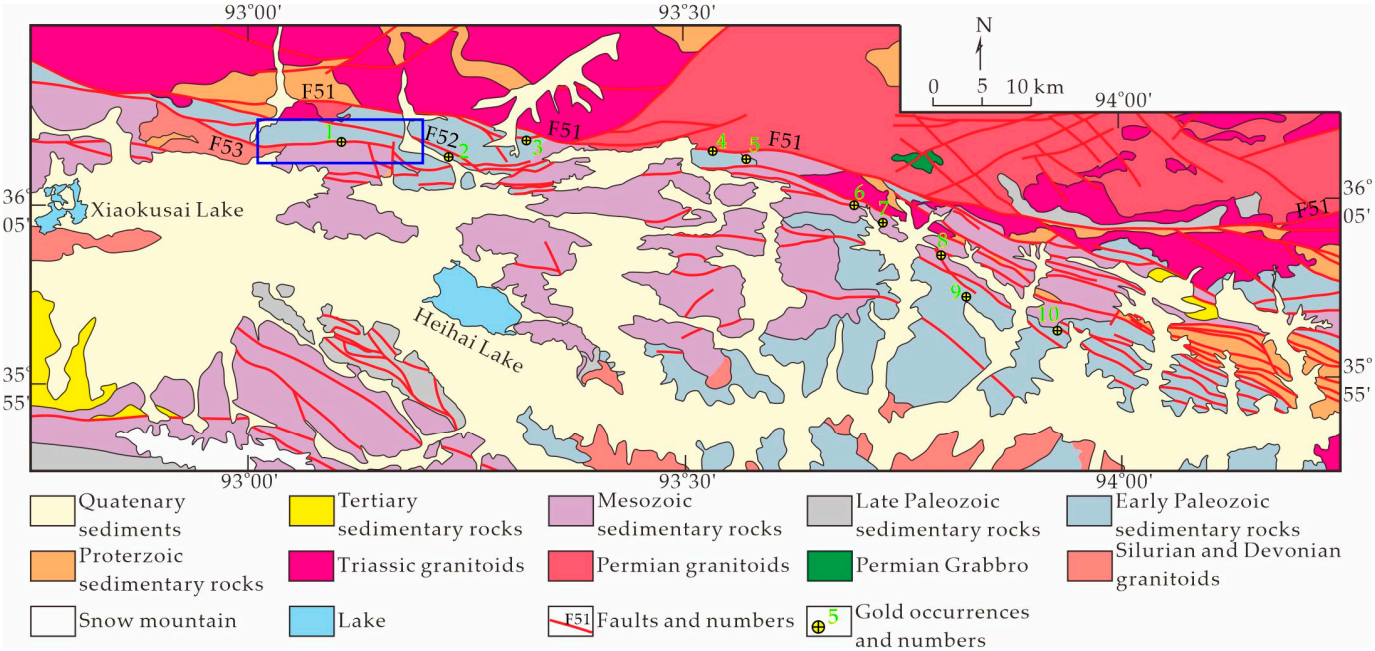


Figure 2. Geological map of the Kunlun River area in EKO (modified after [22]). Numbers and names of gold occurrences: 1—Heiaibei, 2—Lalingzaohuo, 3—Suhaitu, 4—Jiaxi, 5—Xiangyanggou, 6—Jiaodong, 7—Dazaohuo–Heicigou, 8—Dazaohuodong, 9—Yaodongshan, 10—Heicigou.

A systematic study on the H, O, S, and Pb isotope geochemistry for auriferous quartz vein ores in the Heihaibei gold deposit was carried out. Comparing our new data and a few previously published data on the Heihaibei gold deposit, we can better interpret the sources of H, O, S, and Pb in the Heihaibei gold deposit, determine the genetic type of it, and even further constrain the sources of ore-forming fluids and materials for gold deposits within the whole KLRA.

2. Geological Background and Ore Deposit Geology

2.1. Geological Background

Usually, it is thought that the EKO has stages of orogenies that are closely related to the subduction and closure of the Proto-Tethys and Paleo-Tethys oceans [1,3,31–37]. Two ophiolite belts, which lay along the M.KLF and S.KLF–AMF, represent the suture zones of the Neo-Proterozoic to Early Devonian Proto-Tethys, and the Carboniferous to Late Triassic Paleo-Tethys oceans, respectively [3,31,37]. The EKO is considered to be divided into three fault-bounded tectonic belts, i.e., NKL, MKL, and SKL (Figure 1b) [3]. The NKL and MKL have dual tectonic layers of a common Precambrian craton, which are characterized by the Paleo-Proterozoic basement, with intermediate to high-grade metamorphism, and the Meso- to Neo-Proterozoic cover strata, with low-grade metamorphism [2]. The NKL is characterized by thick Ordovician clastic and carbonate sedimentary rocks interlayered with mafic volcanic rocks, which were unconformably overlain by the Devonian molasse sediments [38,39]. Widespread granitoids intruded into these Ordovician and Devonian strata, primarily in the late Paleozoic, in this belt [40,41]. The MKL, in which the Precambrian metamorphic rocks vary from gneiss to schist to phyllite [3,39], was predominantly emplaced by the widespread Neo-Proterozoic, early Cambrian–Early Devonian, and Late Permian–Early Triassic granitic intrusions [13,42–46]. The SKL is dominated by Precambrian to Jurassic siliciclastic and carbonate rocks [3,43], and it was locally intruded upon by the Paleozoic and Triassic granites [23,47,48]. The KLRA is tectonically located in the central segment of the SKL within the EKO (Figure 1b).

2.2. Ore Deposit Geology

The KLRA, as the voluminous area to the north bank of the Kunlun River is usually referred to, is a recently discovered gold mineralization belt in the SKL (Figure 2). The northwest-striking Fault F51, which is a segment of the M.KLF, is a regional fault that bounds the MKL and SKL in the KLRA. To the north of Fault F51, the part of the MKL is characterized by widespread Permian to Triassic granitoids [22]. To the south of Fault F51, part of the SKL is composed of sedimentary rocks which were deposited predominantly in the Early Paleozoic and Quaternary, with minor parts in the Proterozoic and Tertiary. A few Silurian and Triassic granitoids were intruded in the Early Paleozoic and Mesozoic sedimentary rocks (Figure 2). Subsidiary faults of Fault F51 that were usually considered to be the products of the closure of the Proto-Tethys Ocean [49] mostly affect the SKL. Moreover, Fault F51 and its subsidiary faults in the KLRA would have been reactivated from the Early Triassic onwards because of the subduction of the Paleo-Tethys oceanic plate [2,49]. Ore-forming hydrothermal fluids can migrate upward through such reactivated faults. More than 10 gold deposits are controlled by the WNW-striking subsidiary faults to the south of Fault F51 in the KLRA (Figure 2) [22,25].

The Heihaibei gold deposit, which is located ca. 20 km NW of the Heihai Lake, is the westernmost of 10 gold deposits in the KLRA (Figure 3). The dominant sedimentary rocks in the Heihaibei area are mainly composed of Silurian–Ordovician Nachitai Group metamorphic feldspathic quartz sandstone and sandy slate in the north, and Triassic Hongshuichuan Formation feldspathic quartz sandstone in the south, with minor Middle-Neo-Proterozoic Wanbaogou Group sandy limestone and basalt, and Triassic Naocangjiangou Formation feldspathic quartz sandstone in the southeast (Figure 3a) [22,23]. An EW- to WNW-striking >15 km long and >100 m wide monzogranite–granodiorite dyke (i.e., the Heihaibei granites) was intruded along the south of the Silurian–Ordovician Nachitai Group. We argued that this monzogranite–granodiorite dyke was classified as A-type granite [50] and was emplaced in the Early Devonian (416 Ma) in a post-collisional setting [50]), rather than in the Ordovician–Silurian (442 Ma [27]), 443 Ma [25], and 453 Ma [23]). The Triassic Hongshuichuan Formation feldspathic quartz sandstone and other minor Triassic sediments were deposited over older sedimentary rocks and the Heihaibei granites [24]. Subsidiary faults in the Heihaibei area predominantly include the NW-striking Fault F52 and Fault F53 (Figure 3a). Fault F52, ca. 18 km long and 10–100 m wide, generally strikes WNW across the Nachitai Group sandstone in the northeast part of the Heihaibei mining area and dips 25°–52° to the north; meanwhile, Fault F53, ca. 15 km long and 10–100 m wide, generally strikes EW across the central part of the study area and dips 30°–63° to the north [23,24]. Cataclasites, fault breccias, and fault gouges are developed in the faulted zones of Faults F52 and F53. Fault F53 with secondary branch faults, i.e., Fault F53-1, is commonly developed along contacts of different geological bodies in the Heihaibei area, i.e., between the granites and the Triassic Hongshuichuan Formation, and the granites and the Nachitai Group, as well as the slate and sandstone in the Nachitai Group. Some auriferous quartz veins, pyritizations, and weak hydrothermal alterations are developed along the faulted monzogranite zone of Fault F53, but little mineralization occurs in Fault F52, which is limited in the Nachitai Group sandstone (Figure 3b).

Weak hydrothermal alterations within monzogranite wall rocks (Figure 4a) are mostly silicification and sericitization, with minor chloritization and carbonatization. In monzogranites, biotite is basically altered into chlorite, plagioclase is partially altered into muscovite, and hydrothermal quartz and/or calcite fill into fine fractures (Figure 4b,c). More than 20 gold ore bodies (with Au abundances larger than the cut-off grade) and 30 auriferous bodies (with Au abundances below the cut-off grade) were delineated in the faulted monzogranite zone within the fault F53, and they yielded a total reserve of 5.7 t Au, with an average grade of 4.8 g/t, in which the 660 m long and average 5 m wide ore body M3 contributes to ca. 90% of the Au reserves [22]. Most of the gold ore bodies strike EW to ENE (east-northeast) and occur as lenses along the faulted monzogranite zone within Fault F53 (Figures 3b and 5). Ore bodies consist of predominant smoky grey quartz veins

with minor stockwork quartz veinlets or breccias in the altered monzogranite, and smoky grey quartz veins are usually bordered by fault breccia belts in the faulted monzogranite belt [22,24].

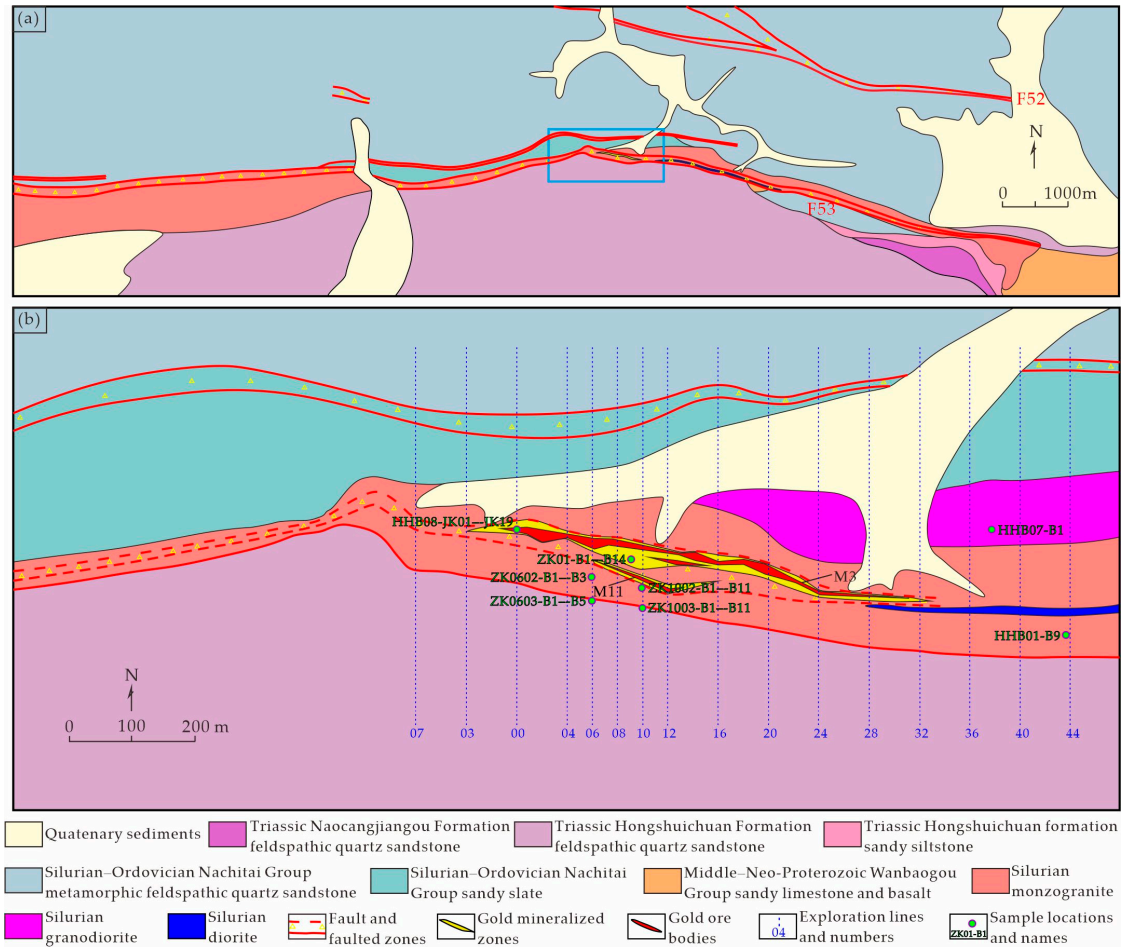


Figure 3. (**a**) Geological map of the Heihaibei and part of Lalingzaohuo area in the KLRA (simplified and revised after [22]). (**b**) Geological map of the Heihaibei gold deposit in the KLRA (simplified and revised after [22]).

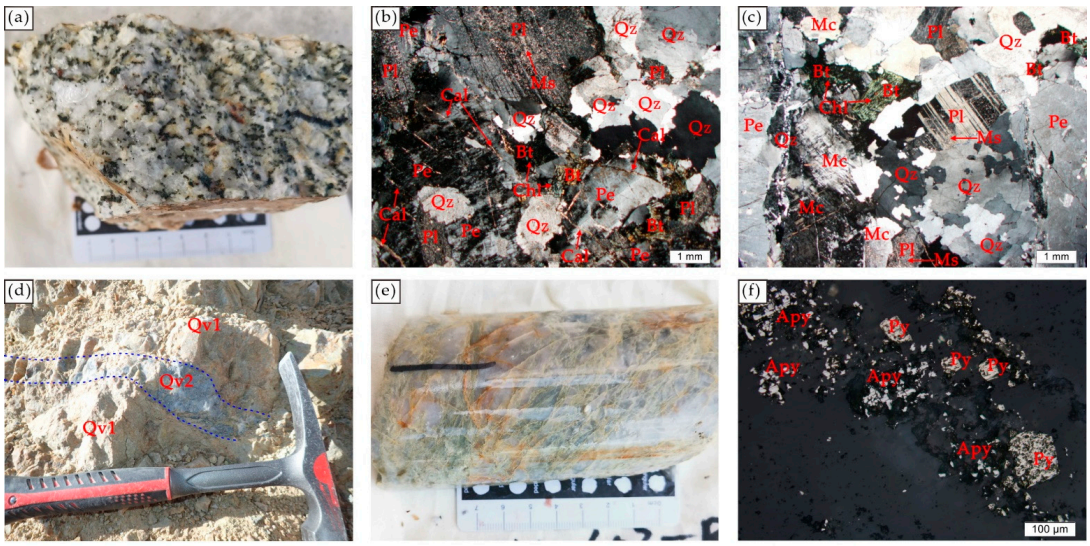


Figure 4. *Cont.*

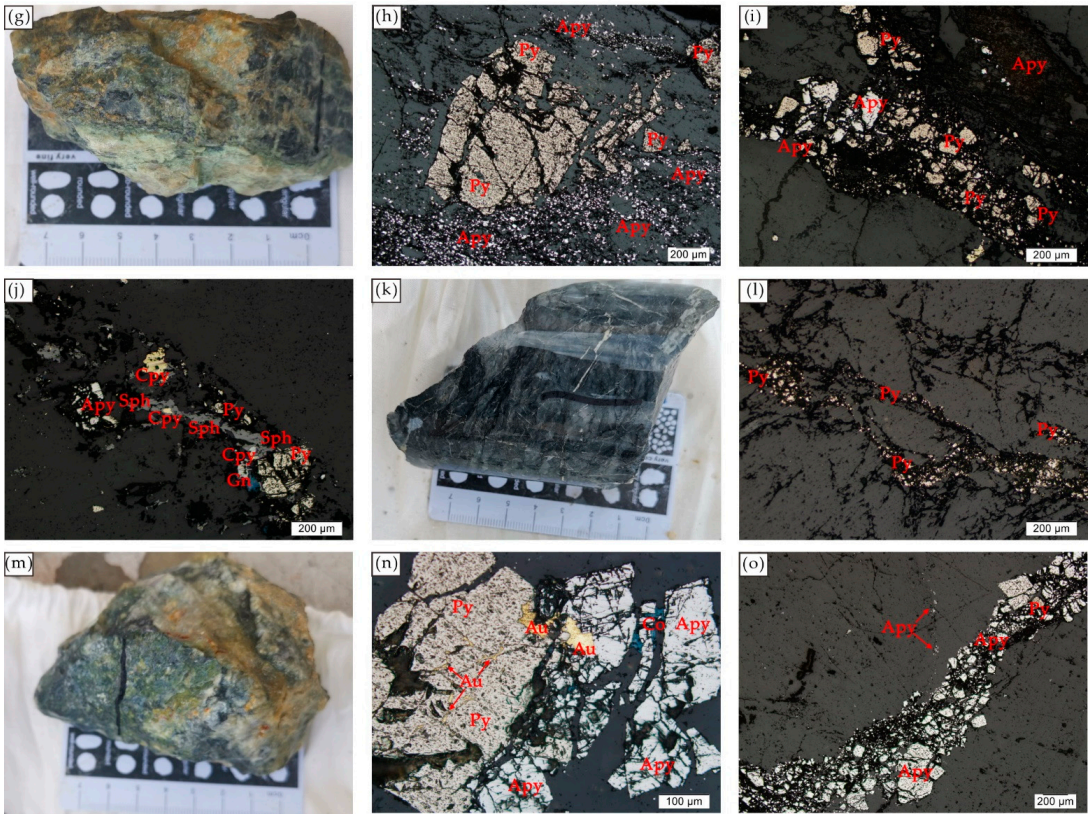


Figure 4. Photographs and photomicrographs showing the morphologies and textural features of the ores and monzogranite wall rocks in the Heihaibei gold deposit. Photo (**a**) and photomicrographs (**b**,**c**) of monzogranite wall rock sample with weak hydrothermal alterations; (**d**) photograph of quartz veins, white quartz veins (Qv1) were cut by a smoky grey quartz vein (Qv2); (**e**) photograph and (**f**) photomicrograph of Qv1 type sample HHBZK0602-B2; (**g**) photograph and (**h**) photomicrograph of Qv2 type sample HHB08-JK11; (**i**,**j**) photomicrographs of typical Qv2 type samples; (**k**) photograph and (**l**) photomicrograph of samples HHBZK1003-B11 from breccia ores; (**m**) photograph and photomicrograph (**n**,**o**) of Qv2 type sample HHB08-JK13. Apy—arsenopyrite, Py—pyrite, Gn—galena, Sph—sphalerite, Cpy—chalcopyrite, Au—native gold, Co—covellite, Mc—microcline, Pe—perthite, Pl—plagioclase, Bt—biotite, Ms—muscovite, Chl—chlorite, Qz—quartz, Cal—calcite.

Three mineralized stages were proposed in the Heihaibei gold deposit, i.e., the K-feldspar-quartz-pyrite-arsenopyrite-sericite-epidote (I), the quartz-pyrite-native gold-chlorite (II), and the quartz-carbonate (III) by [23]. Based on the field survey and the optical microscopic study, we argued that the so-called K-feldspar-quartz-pyrite-arsenopyrite-sericite-epidote stage (I) represents silicified granites with few pyrite veinlets, and that the K-feldspar in such ores is a primary rock-forming mineral rather than a hydrothermal mineral in the Heihaibei granites. Additionally, we cannot find any typical products (e.g., quartz calcite veins) of the so-called quartz-carbonate stage (III) in the ore deposit. Therefore, we considered that the paragenetic sequences in the Heihaibei gold deposit might be divided into three major stages, i.e., the hydrothermal stage, the deformation stage, and the supergene stage (Figure 6). The hydrothermal stage can be subdivided into the sulfide–poor–quartz epoch (I) and the polymetallic–sulfide–quartz epoch (II). A few white quartz veins (here called Qv1), which are composed of predominant quartz with minor sericite, pyrite, and arsenopyrite, represent the sulfide–poor–quartz ore epoch (I) (Figure 4e,f), and some white quartz veinlets or silicification in weakly altered monzogranite wall rocks (Figure 4b,c) are the products of this epoch. Predominant smoky grey quartz veins (here called Qv2), which represent the ores from the polymetallic–sulfide–quartz epoch (II), usually contain predominant quartz with a few sulfide veinlets, disseminations, or massive aggregations, which consist of pyrite and arsenopyrite, with minor native gold,

chalcopyrite, galena, sphalerite, and tetrahedrite (Figure 4g–j,m–o). Micro-native gold is mostly trapped in pyrite, and arsenopyrite in the Qv2 (Figure 4n). Usually, the contents of sulfides in the Qv2 are less than 5%. Some pyrite–quartz-bearing veinlets and stockworks, which can be found in the weakly altered monzogranite wall rock or Qv1, constitute gold mineralized zones, and some of them may be delineated to ore bodies. Comparatively, the sulfide–poor–quartz epoch (I) and polymetallic–sulfide–quartz epoch (II) in this study are roughly referred to as the stage I and stage II, respectively, as classified by [23]. Partially, both Qv1 and Qv2 can be deformed within the faulted monzogranite zone of Fault F53 and become breccia ores (Figure 4k,l). The oxidized ores from the supergene stage mostly consist of goethite, lepidocrocite, and covellite, which result from the replacement of the hydrothermal stage of primary Qv1 and Qv2 (Figures 4n and 6). In a word, the geological characteristics of the Heihaibei gold deposit show similar features to those of the orogenic gold deposits defined by [51].

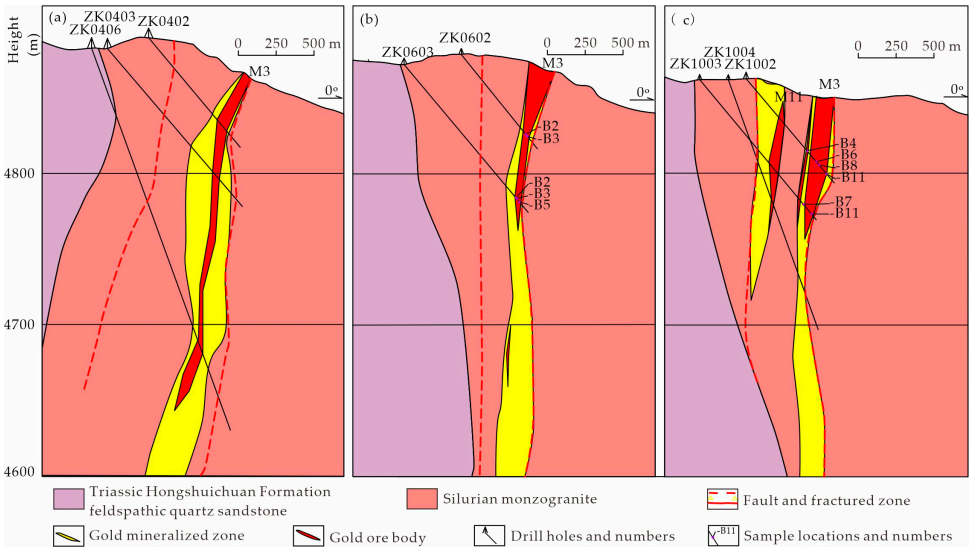


Figure 5. Typical sections of the Heihaibei gold deposit (Simplified and revised from [22]). (**a**) Prospecting line 4, (**b**) Prospecting line 6, (**c**) Prospecting line 8.

Stages / Minerals	Hydrothermal stage		Deformation Stage	Supergene Stage
	Sulfide–Poor–Quartz epoch (I)	Polymetallic–Sulfide–Quartz Epoch (II)		
pyrite	—	—		
Arsenopyrite	—	—		
Native Gold		—		
Calcopyrite		—		
Sphalerite		—		
Galena		—		
Tetrahedrite		—		
Quartz	—	—		
Sericite	—	—	—	
Chlorite		—	—	
Calcite		—	—	
Goethite				—
Lepidocrocite				—
Covellite				—

Figure 6. Paragenetic sequences of minerals in different ore-forming stages in the Heihaibei gold deposit. The length and width of the square represent the time and amount of mineral growth, respectively.

3. Sampling and Analytical Methods

3.1. Sampling

The samples for isotope analyses were collected from drill cores, i.e., ZK0602, ZK0603, ZK01, ZK1002, and ZK1003, or surface outcrop sites, i.e., HHB01, HHB07, and HHB08. Detailed sample locations and numbers can be found in Figures 3b and 5, and Table 1. Fifteen auriferous quartz samples (Qv1 and Qv2) were collected for oxygen and hydrogen isotope analysis (Table 2). Seventeen sulfide-bearing ore samples (Qv1 and Qv2) were collected for sulfur isotope analysis (Table 3). Four sulfide-bearing ore samples (Qv1 and Qv2) and five potassic feldspars in the Heihaibei granites were collected for lead isotope analysis (Table 4). Previously published data for other gold deposits in the EKO, compared with data in this study, can be found in the Supplementary Materials (Tables S1–S3).

Table 1. Sample list in the Heihaibei gold deposit.

No.	Sample Name	Rock Type	Ore Type	Mineral Assembly	Location
1	HHBZK0602-B2	brecciated white quartz vein	Qv1	quartz with minor sericite, pyrite, and arsenopyrite	69.7 m of the drillhole core of the ZK1002
2	HHBZK1002-B4	brecciated white quartz vein	Qv1		62.9 m of the drillhole core of the ZK1004
3	HHBZK1002-B6	brecciated white quartz vein	Qv1		72.3 m of the drillhole core of the ZK1004
4	HHBZK1002-B8	brecciated white quartz vein	Qv1		75.5 m of the drillhole core of the ZK1004
5	HHB08-JK01	white quartz vein	Qv1		93°06′39″ E, 36°08′35″ N
6	HHB08-JK10	white quartz vein	Qv1		93°06′39″ E, 36°08′35″ N
7	HHB08-JK17	white quartz vein	Qv1		93°06′39″ E, 36°08′35″ N
8	HHBZK01-B3	brecciated smoky grey quartz vein	Qv2	quartz with some pyrite and arsenopyrite, and minor native gold, chalcopyrite, galena, and sphalerite, as well as tetrahedrite	26.4 m of the drillhole core of the ZK01
9	HHBZK01-B5	brecciated smoky grey quartz vein	Qv2		29.6 m of the drillhole core of the ZK01
10	HHBZK01-B6	brecciated smoky grey quartz vein	Qv2		30.3 m of the drillhole core of the ZK01
11	HHBZK0602-B3	smoky grey quartz vein	Qv2		70.8 m of the drillhole core of the ZK0602
12	HHBZK0603-B2	smoky grey quartz vein	Qv2		114.7 m of the drillhole core of the ZK0603
13	HHBZK0603-B3	brecciated smoky grey quartz vein	Qv2		115.4 m of the drillhole core of the ZK0603
14	HHBZK0603-B5	brecciated smoky grey quartz vein	Qv2		117.0 m of the drillhole core of the ZK0603
15	HHBZK1003-B11	brecciated smoky grey quartz vein	Qv2		115.9 m of the drillhole core of the ZK1003
16	HHBZK1002-B11	brecciated smoky grey quartz vein	Qv2		82.8 m of the drillhole core of the ZK1002
17	HHB08-JK02	smoky grey quartz vein	Qv2		93°06′39″ E, 36°08′35″ N
18	HHB08-JK03	smoky grey quartz vein	Qv2		93°06′39″ E, 36°08′35″ N
19	HHB08-JK05	smoky grey quartz vein	Qv2		93°06′39″ E, 36°08′35″ N
20	HHB08-JK08	smoky grey quartz vein	Qv2		93°06′39″ E, 36°08′35″ N
21	HHB08-JK13	smoky grey quartz vein	Qv2		93°06′39″ E, 36°08′35″ N
22	HHB08-JK15	smoky grey quartz vein	Qv2		93°06′39″ E, 36°08′35″ N
23	HHB08-JK18	smoky grey quartz vein	Qv2		93°06′39″ E, 36°08′35″ N
24	HHB08-JK19	smoky grey quartz vein	Qv2		93°06′39″ E, 36°08′35″ N
25	HHBZK01-B11	monzogranite	wall rock	plagioclase, 25–40% alkali feldspar, 25–45% quartz, <5% biotite	175.0 m of the drillhole core of the ZK01
26	HHB01-B9	monzogranite	wall rock		93°07′14″ E, 36°08′30″ N
27	HHBZK01-B14	granodiorite	wall rock	35–50% plagioclase, 35–45% quartz, 10–15% alkali feldspar, <5% biotite	209.4 m of the drillhole core of the ZK01
28	HHBZK1003-B7	granodiorite	wall rock		107.2 m of the drillhole core of the ZK1003
29	HHB07-B1	granodiorite	wall rock		93°07′09″ E, 36°08′36″ N

Table 2. H and O isotope data for quartz in the Heihaibei gold deposit. δD was measured in fluid inclusions; $\delta^{18}O$ was measured in quartz; $\delta^{18}O$ of water in equilibrium with quartz was calculated at the temperature indicated by Th [23] using the equation of $1000\ln\alpha = 3.38 \times 10^6/T^2 - 3.4$ [52].

No.	Sample Name	Rock Type	Ore Type	Mineral	δDVSMOW (‰)	δ^{18}OVSMOW (‰)	δ^{18}OH2O (‰)	Average Th (°C)	References
1	HHBZK0602-B2	brecciated white quartz vein	Qv1	Quartz	−97.2	13.4	7.8	340.0	this study
2	HHBZK0602-B3	smoky grey quartz vein	Qv2	Quartz	−91.0	12.1	2.7	241.0	this study
3	HHBZK0603-B2	smoky grey quartz vein	Qv2	Quartz	−101.8	12.6	3.2	241.0	this study
4	HHBZK0603-B3	brecciated smoky grey quartz vein	Qv2	Quartz	−97.7	12.8	3.4	241.0	this study
5	HHBZK0603-B5	brecciated smoky grey quartz vein	Qv2	Quartz	−102.3	13.3	3.9	241.0	this study
6	HHB08-JK01	white quartz vein	Qv1	Quartz	−81.1	9.2	3.6	340.0	this study
7	HHB08-JK02-1	smoky grey quartz vein	Qv2	Quartz	−94.1	13.7	4.3	241.0	this study
8	HHB08-JK02-2	smoky grey quartz vein	Qv2	Quartz	−94.6	13.7	4.3	241.0	this study
9	HHB08-JK03	smoky grey quartz vein	Qv2	Quartz	−89.9	11.3	1.9	241.0	this study
10	HHB08-JK05	smoky grey quartz vein	Qv2	Quartz	−90.4	13.6	4.2	241.0	this study
11	HHB08-JK08	smoky grey quartz vein	Qv2	Quartz	−97.4	11.6	2.2	241.0	this study
12	HHB08-JK10	white quartz vein	Qv1	Quartz	−92.8	13.9	8.3	340.0	this study
13	HHB08-JK15	smoky grey quartz vein	Qv2	Quartz	−97.6	11.6	2.2	241.0	this study
14	HHB08-JK17	white quartz vein	Qv1	Quartz	−96.8	11.0	5.4	340.0	this study
15	HHB08-JK18	smoky grey quartz vein	Qv2	Quartz	−104.2	13.0	3.6	241.0	this study
16	HHB08-JK19	smoky grey quartz vein	Qv2	Quartz	−101.5	11.0	1.6	241.0	this study
17	K1	silicified monzogranite	Qv1+wall rocks	Quartz	−84.1	15.1	9.5	340.0	[23]
18	K5	smoky grey quartz vein	Qv2	Quartz	−81.1	14.1	4.7	241.0	[23]
19	K7	smoky grey quartz vein	Qv2	Quartz	−84.0	14.0	4.6	241.0	[23]

Table 3. Sulfur isotope data for sulfides in the Heihaibei deposit. $\delta^{34}S_{H2S}$ means $\delta^{34}S_{VCDT}$ values for H_2S in equilibrium with sulfides. The assumed temperatures of equilibrium for different ore types are the same as Th [23] listed in Table 1.

No.	Sample Name	Rock Type	Ore Type	Mineral	$\delta^{34}S_{CDT}$(‰)	$\delta^{34}S_{H2S}$(‰)	References
1	HHBZK01-B3	brecciated smoky grey quartz vein	Qv2	Pyrite	8.5	7.0	this study
2	HHBZK01-B5	brecciated smoky grey quartz vein	Qv2	Pyrite	8.0	6.5	this study
3	HHBZK01-B6	brecciated smoky grey quartz vein	Qv2	Pyrite	7.7	6.2	this study
4	HHBZK0603-B2	smoky grey quartz vein	Qv2	Pyrite	8.0	6.5	this study
5	HHBZK0603-B3	brecciated smoky grey quartz vein	Qv2	Pyrite	7.6	6.1	this study
6	HHBZK0603-B5	brecciated smoky grey quartz vein	Qv2	Pyrite	8.0	6.5	this study
7	HHBZK1003-B11	brecciated smoky grey quartz vein	Qv2	Pyrite	7.6	6.1	this study

Table 3. *Cont.*

No.	Sample Name	Rock Type	Ore Type	Mineral	$\delta^{34}S_{CDT}$(‰)	$\delta^{34}S_{H2S}$(‰)	References
8	HHBZK1002-B4-1	brecciated white quartz vein	Qv1	Pyrite	8.1	7.0	this study
9	HHBZK1002-B4-2	brecciated white quartz vein	Qv1	Pyrite	8.0	6.9	this study
10	HHBZK1002-B6	brecciated white quartz vein	Qv1	Pyrite	8.0	6.9	this study
11	HHBZK1002-B8	brecciated white quartz vein	Qv1	Pyrite	8.1	7.0	this study
12	HHBZK1002-B11	brecciated smoky grey quartz vein	Qv2	Pyrite	7.8	6.3	this study
13	HHB08-JK02	smoky grey quartz vein	Qv2	Pyrite	8.5	7.0	this study
14	HHB08-JK08	smoky grey quartz vein	Qv2	Pyrite	8.0	6.5	this study
15	HHB08-JK13	smoky grey quartz vein	Qv2	Pyrite	8.3	6.8	this study
16	HHB08-JK15	smoky grey quartz vein	Qv2	Pyrite	8.2	6.7	this study
17	HHB08-JK17	white quartz vein	Qv1	Pyrite	8.7	7.6	this study
18	K1	silicified monzogranite	Qv1 + wall rocks	Arsenopyrite	8.5		[23]
19	K5	smoky grey quartz vein	Qv2	Pyrite	7.7		[23]
20	K8	smoky grey quartz vein	Qv2	Pyrite	7.9		[23]

Table 4. Pb isotope compositions for sulfides in the Heihaibei gold deposit.

No.	Sample	Rock Type	Ore Type	Mineral	$^{206}Pb/^{204}Pb$	$^{207}Pb/^{204}Pb$	$^{208}Pb/^{204}Pb$	References
1	HHBZK01-B3	brecciated smoky grey quartz vein	Qv2	pyrite	18.8122	15.7002	38.8055	this study
2	HHBZK1002-B4	brecciated white quartz vein	Qv1	pyrite	19.0007	15.7062	38.7655	this study
3	HHB08-JK08	smoky grey quartz vein	Qv2	pyrite	18.7219	15.6959	38.7356	this study
4	HHB08-JK19	smoky grey quartz vein	Qv2	pyrite	18.8262	15.6998	38.7836	this study
5	HHBZK01-B11	monzogranite	wall rock	K-feldspar	18.4283	15.6789	38.4342	this study
6	HHBZK01-B14	granodiorite	wall rock	K-feldspar	18.4363	15.6808	38.4532	this study
7	HHBZK1003-B7	granodiorite	wall rock	K-feldspar	18.4864	15.6475	38.1750	this study
8	HHB01-B9	monzogranite	wall rock	K-feldspar	18.4368	15.6812	38.4598	this study
9	HHB07-B1-1	granodiorite	wall rock	K-feldspar	18.3532	15.6750	38.3713	this study
10	HHB07-B1-2	granodiorite	wall rock	K-feldspar	18.3537	15.6753	38.3724	this study
11	K1	silicified monzogranite	Qv1 + wall rocks	pyrite	19.188	15.713	39.235	[23]
12	K5	smoky grey quartz vein	Qv2	pyrite	18.722	15.695	38.728	[23]
13	K12	smoky grey quartz vein	Qv2	pyrite	18.724	15.699	38.746	[23]

3.2. Oxygen and Hydrogen Isotope Analysis

Oxygen isotope analyses were carried out with the bromine pentafluoride method of [53] at the Key Laboratory of Metallogeny and Mineral Assessment, Institute of Mineral Resources, Chinese Academy of Geological Sciences (CAGS), China. Oxygen was liberated from 6 mg of quartz via reaction with BrF_5 and converted to CO_2 on a platinum-coated carbon rod. The $\delta^{18}O$ determinations were made on a Thermo Scientific 253 plus mass spectrometer, with analytical precisions of ±0.2‰, and the detailed analytical procedures are described by [54]. Hydrogen isotope analyses were carried out at the Beijing Createch Testing Technology Co., Ltd, Beijing, China (BCTT). Hydrogen isotopic ratios were measured on water released via decrepitation (at 1420 °C), of crushed and sieved (to the size range of 60 mesh) 10–20 mg quartz, according to the method of [55]. Samples were first degassed by heating under a vacuum at 90 °C for 12 h; then, the water was released from fluid inclusions by heating the samples to 1420 °C in a Thermo Scientific Flash 2000 HT elemental analyzer. The subsequently released water was trapped, reduced to H_2 by glassy carbon, and then analyzed for δD values using a Thermo Scientific 253 plus mass spectrometer, with a precision of ±1‰. The isotope results are expressed in the delta (δ) notation as the per mil (‰) deviation relative to the Vienna Standard Mean Ocean Water (V-SMOW) standard. The isotopic fractionation of oxygen between quartz and water was calculated using the equation of $1000\ln\alpha = 3.38 \times 10^6/T^2 - 3.4$ [52].

3.3. Sulfur Isotope Analysis

Sulfur isotope analyses of sulfide separates were carried out at BCTT using the conventional combustion method [56]. The detailed analytical procedures are described by [57]. Approximately 15 mg of sulfides were combusted at 960 °C for quantitative conversion to SO_2, which were then analyzed for sulfur isotope with a Thermo Scientific 253 plus mass spectrometer. The results are reported in the δ notation as the ‰ deviation of the isotope ratio ($^{34}S/^{32}S$) relative to the Vienna Canyon Diablo Troilite (V-CDT) standard, with an analytical precision of ± 0.2‰.

3.4. Lead Isotope Analysis

Lead isotope analyses were conducted on four pyrite separates and five potassic feldspar separates at BCTT, using the analytical procedure as described in [58]. About 150 mg of the pyrite or feldspar sample were completely dissolved in an ultrapure acid mixture of 1 mL HNO_3 + 2 mL HF. After drying, the residue was redissolved in concentrated HNO_3 and dried again. Finally, the sample residue was dissolved in 1mL 3.5 M HNO_3 and then loaded into a column with 100–150 μm of Triskem Sr-Spec resins to separate the Pb fraction by washing with 3.5 M HNO_3, 8 M HCl, and Milli-Q water. Finally, the extracted sample residue was dissolved in 1 mL 2% HNO_3. Isotopic ratios of Pb analyses were undertaken using a Thermo Scientific Neptune Plus Multi Collector-Inductively Coupled Plasma Mass Spectrometer (MC-ICP-MS), and the results were corrected using $^{203}Tl/^{205}Tl = 0.418922$ [58]. The data quality was monitored via repeated analyses of the CAGS Pb reference material, and the error margin (2σ) was <0.002 for all three ratios.

4. Results

4.1. Oxygen and Hydrogen Isotope Results

Quartz samples from quartz veins show a $\delta^{18}O_{quartz}$ range from +9.2 to +13.9‰, with an average of +12.3‰ (Table 2, Figure 7). It is difficult to calculate the precise $\delta^{18}O_{H2O}$ values of fluids that were in equilibrium with quartz, due to a large variation of temperatures [23] obtained from fluid inclusions (e.g., [59]). According to the microthermometry of fluid inclusions in auriferous quartz from the Heihaibei gold deposit finished by [23], the homogenization temperatures of Qv1 type of quartz from epoch I range from 268 °C to 412 °C, with an average of 340 °C; meanwhile, the homogenization temperatures of the Qv2 type of quartz from epoch II range from 183 °C to 288 °C, with an average of 241 °C. Usually,

the trapping temperature could be defined by the average homogenization temperature to calculate the isotopic fractionation values. Given 340 °C as the trapping temperature for epoch I, the $\delta^{18}O_{H2O}$ values of the ore-forming fluids in the fluid inclusions from the quartz in the Qv1 samples range from +3.6‰ to +8.3‰ (Table 2, Figure 7b). Meanwhile, given 241 °C as the trapping temperature for epoch II, the $\delta^{18}O_{H2O}$ values of the ore-forming fluids for fluid inclusions from quartz in the Qv2 samples range from +1.6‰ to +4.3‰ (Table 2, Figure 7b). Generally, the trapping temperatures are most likely higher than the homogenization temperatures for the orogenic fluids.

The hydrogen isotope results for the fluid inclusions from the quartz samples are also shown in Table 2, in which the δD_{VSMOW} values range from −104.2‰ to −81.1‰, with an average of −95.3‰ (Figure 7). The quartz in the Qv1 samples has δD_{VSMOW} values ranging from −97.2 ‰ to −81.1‰, and the quartz in the Qv2 samples has δD_{VSMOW} values ranging from −104.2‰ to −89.9‰ (Figure 7b).

Consequently, the analytical hydrogen isotopes and the calculated $\delta^{18}O_{H2O}$ values for the fluid inclusions from the quartz in Qv1 and Qv2 samples are different from each other (Figure 7b). Three sets of hydrogen–oxygen isotope compositions for the Heihaibei gold deposits were previously reported by [23], in which two samples from the smoky grey quartz veins (Qv2) have similar hydrogen–oxygen isotope compositions as our data from Qv1. However, the sample K1 is slightly different from our data from Qv1, likely because it might have been collected in the mineralized Heihaibei granitic wall rock, thus representing a mixed sample of Qv1 plus the granitic wall rock.

4.2. Sulfur Isotope Results

Only pyrite separates had been selected from 16 ore samples and analyzed for sulfur isotope compositions. Other sulfide separates were insufficient for analysis because the ore samples were collected from drill cores and had limited volumes. The $\delta^{34}S_{VCDT}$ values of 17 pyrite separates from 16 ore samples in the Heihaibei gold deposit range from +7.6‰ to +8.7‰, with a narrow variation and an average of 8.1‰ (Table 3, Figure 8a). Pyrite separates from the Qv1 type of ores have almost invariable $\delta^{34}S$ values ranging from +8.0‰ to +8.7‰, with an average of + 8.2‰. Pyrite separates from the Qv2 type of ores have similar invariable $\delta^{34}S$ values ranging from +7.6‰ to +8.5‰, with an average of +8.0‰. The $\delta^{34}S$ values of all pyrites have very narrow variations, and the $\delta^{34}S$ values of different ores have a comparably small range, usually indicating a relatively unique source.

Furthermore, our sulfur isotope data, ranging from +7.6‰ to +8.7‰, essentially coincide with the three previously published $\delta^{34}S_{VCDT}$ values, i.e., +7.7‰, +7.9‰, and +8.5‰ [23].

4.3. Lead Isotope Results

Only four pyrites separated from four ore samples in the Heihaibei gold deposit were large enough and yielded relatively invariable Pb isotope compositions, with $^{206}Pb/^{204}Pb$ ratios of 18.7219 to 19.0007, $^{207}Pb/^{204}Pb$ ratios of 15.6959 to 15.7062, and $^{208}Pb/^{204}Pb$ ratios of 37.7359 to 38.8055 (Table 4, and Figure 9a,b). Different types of quartz veins have relatively similar Pb isotopic compositions (Figure 9c,d). One pyrite separate from the Qv1 type of ores has $^{206}Pb/^{204}Pb$ ratios of 19.0007, $^{207}Pb/^{204}Pb$ ratios of 15.7062, and $^{208}Pb/^{204}Pb$ ratios of 38.7655. Three pyrite separates from the Qv2 type of ores have invariable Pb isotopic ratios, with $^{206}Pb/^{204}Pb$ ratios from 18.7219 to 18.8262, $^{207}Pb/^{204}Pb$ ratios from 15.6959 to 15.7002, and $^{208}Pb/^{204}Pb$ ratios from 38.7356 to 38.8055. Three sets of Pb isotope compositions for the Heihaibei gold deposits have previously been reported by [23], in which two samples from smoky grey quartz veins (Qv2) have similar Pb compositions as our data from Qv2, but the sample K1 has more radiogenic Pb isotope than our data from Qv1.

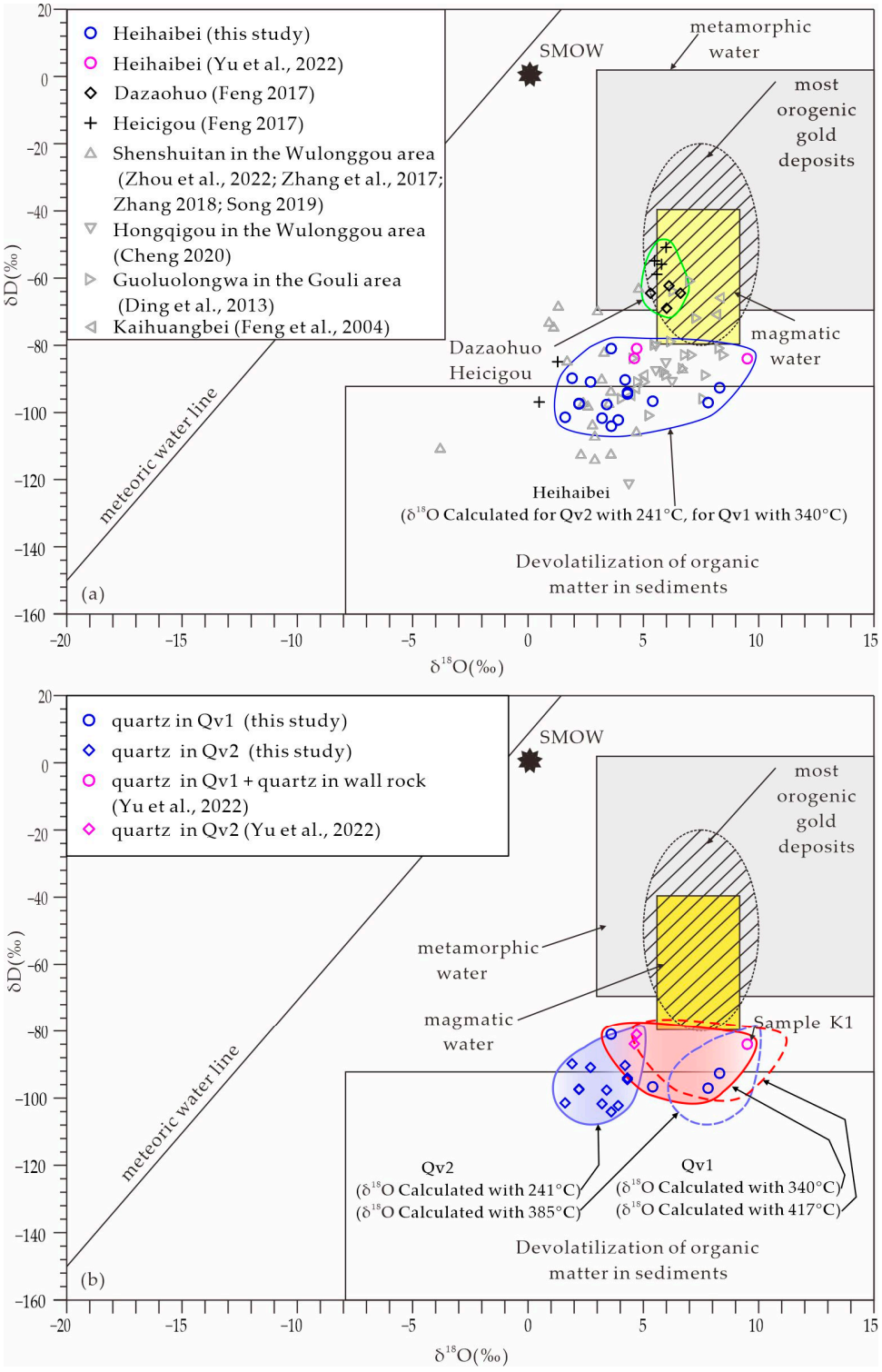


Figure 7. (**a**) Plot of analytical δD $_{VSMOW}$ vs. calculated $\delta^{18}O_{H2O}$ for ore-forming fluids from auriferous quartz veins (for equilibrium at 241 °C for Qv2, 340 °C for Qv1) in the Heihaibei gold deposit, compared with quartz in other gold deposits (data after [4,8–10,14,19,23,29,60], Table S1) in the EKO; (**b**) Plot of analytical δD vs. calculated $\delta^{18}O_{H2O}$ (with homogenization temperatures of 241 °C for Qv2 and 340 °C for Qv1, comparing with arsenopyrite geothermometer temperatures of 385 °C for Qv2 and 417 °C for Qv1) for ore-forming fluids from auriferous quartz veins in the Heihaibei gold deposit. Magmatic, metamorphic, and organic (e.g., devolatilization of organic matter in sediments) water fields after [61]; field for most orogenic gold deposits revised after [59].

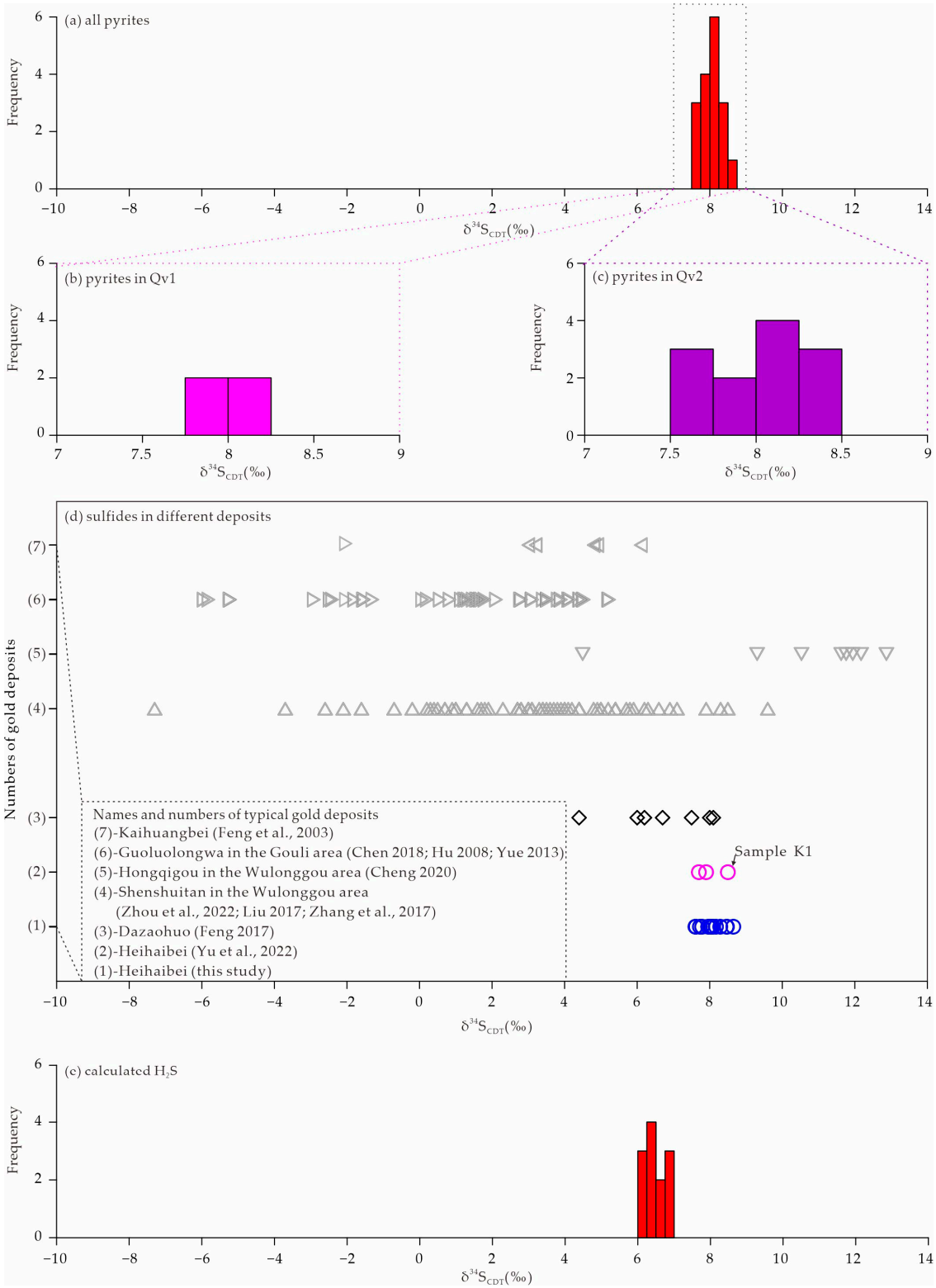


Figure 8. Sulfide isotope for sulfide separates from auriferous quartz veins in the Heihaibei gold deposit. (**a**) Histogram of sulfur isotopes for pyrites from all types of ores; (**b**) Histogram of sulfur isotopes for pyrites in Qv1 type of ores; (**c**) Histogram of sulfur isotopes for pyrites in Qv2 type of ores; (**d**) Plot of sulfur isotopes for sulfides in the Heihaibei gold deposit compared with those in other gold deposits (data after [4,7,9,15–17,20,23,29,60], Table S2) in the EKO; (**e**) Histogram of calculated H_2S isotopes ($\delta^{34}S_{H2S}$) in equilibrium with sulfides in the Heihaibei gold deposit. The assumed temperatures of equilibrium for different ore types are the same as Th [23] listed in Table 1.

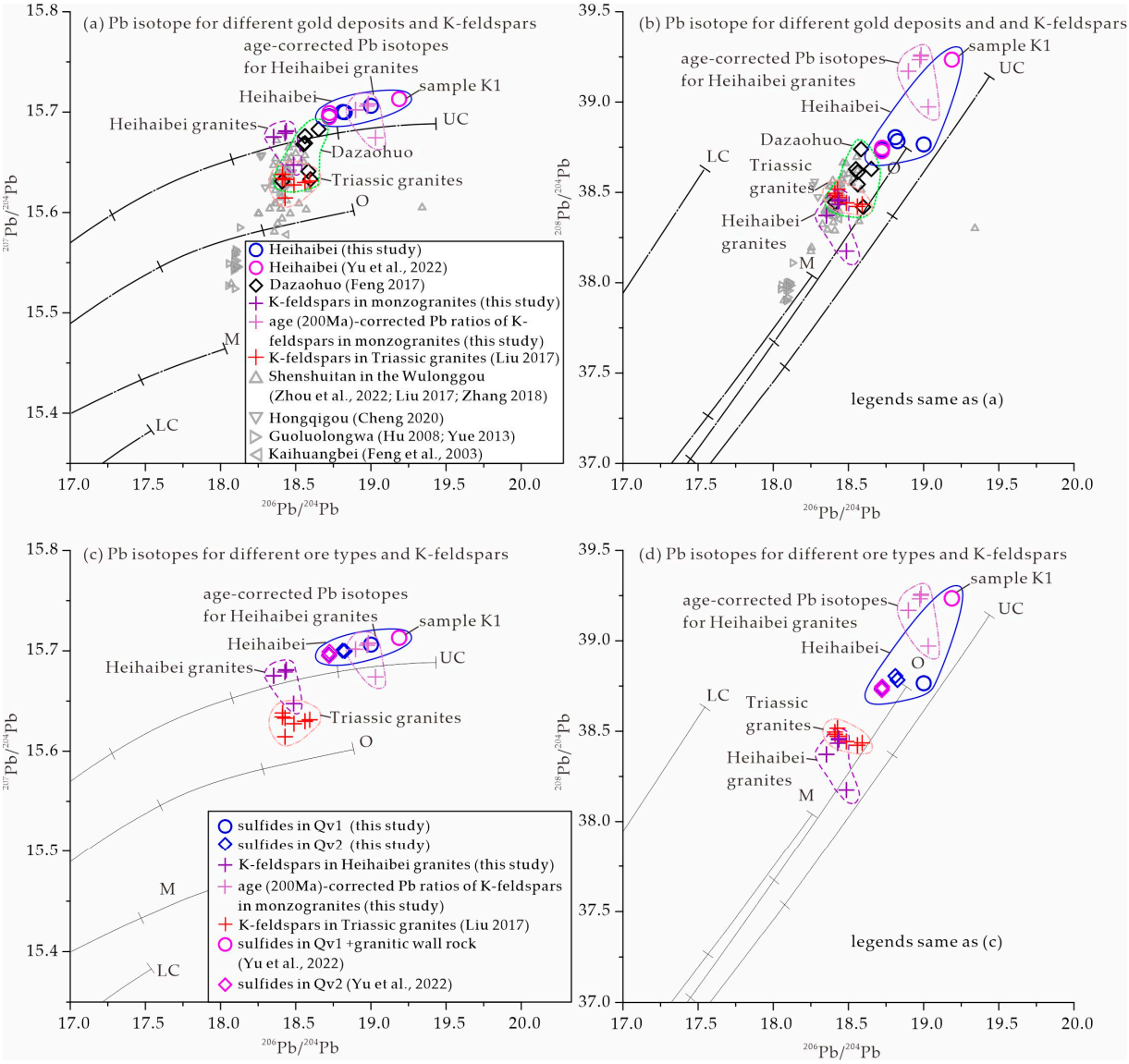


Figure 9. Lead isotopic compositions of sulfide separates in auriferous quartz veins (Qv1 and Qv2), K-feldspars in granite wall rocks, and age (200 Ma)-corrected Pb ratios of K-feldspars in monzogranites in the Heihaibei gold deposit. (**a**) Diagram of $^{207}Pb/^{204}Pb$ vs. $^{206}Pb/^{204}Pb$; (**b**) Diagram of $^{208}Pb/^{204}Pb$ vs. $^{206}Pb/^{204}Pb$ for pyrites and K-feldspars in the Heihaibei gold deposit, compared with sulfides in other gold deposits (data after [4,7,9,16,17,20,23,29,60], Table S3) in the EKO; (**c**) Diagram of $^{207}Pb/^{204}Pb$ vs. $^{206}Pb/^{204}Pb$; and (**d**) Diagram of $^{208}Pb/^{204}Pb$ vs. $^{206}Pb/^{204}Pb$ for different ores compared with K-feldspars in granite wall rocks in the Heihaibei gold deposit. UC, Upper crust; O, Orogen; M, Mantle; LC, Lower crust. The average growth curve is from [62], and tick marks along each curve indicate progressively older times in 0.4 b.y. increments.

Six potassic feldspar separates from five Heihaibei granite wall rocks have invariable Pb isotope compositions, with $^{206}Pb/^{204}Pb$ ratios of 18.3532 to 19.4864, $^{207}Pb/^{204}Pb$ ratios of 15.6475 to 15.6812, and $^{208}Pb/^{204}Pb$ ratios of 37.1750 to 38.4598, indicating the initial lead isotope for the granite wall rocks when they were emplaced at ca. 416 Ma [50].

5. Discussion

5.1. Origins of the Ore-Forming Fluid

The $\delta^{18}O_{VSMOW}$ values (+9.2–+13.9‰) of quartz separates from quartz veins at the Heihaibei gold deposit are basically similar to those of the Phanerozoic orogenic gold

deposits elsewhere ($\delta^{18}O$ = +7–+13‰, [63,64]). Given the average homogenization temperatures of 340 °C and 241 °C as the trapping temperature for the Qv1 and Qv2 samples, the calculated $\delta^{18}O_{H2O}$ values of the fluids in epoch I and epoch II show relatively large variations, from +3.6 to +8.3‰ and +1.6 to +4.3‰, respectively (Table 2, the solid contour lines in Figure 7b). Generally, the trapping temperatures are most likely higher than the homogenization temperatures for the ore-forming fluids. Therefore, the calculated $\delta^{18}O_{H2O}$ values of the fluids would be slightly higher than the values of +1.6–+8.3‰ in the Heihaibei gold deposit. In this regard, application of the arsenopyrite geothermometer, calculated using our unpublished electron microprobe analysis (EMPA) data, even higher average temperatures of 417 °C are obtained for epoch I and 385 °C for epoch II, which could also roughly represent the trapping temperature for the pyrite + arsenopyrite assembly in the Qv1 and Qv2, respectively. Given 417 °C and 385 °C as the trapping temperatures for Qv1 and Qv2, the calculated $\delta^{18}O_{H2O}$ values of the fluids in epoch I and epoch II would be obviously higher than the previously calculated ones, and they would be up to +5.5–+10.2‰ and +6.6–+9.3‰, respectively (the dashed contour lines in Figure 7b). Sheppard (1986) indicates that the $\delta^{18}O_{H2O}$ values for fluids of magmatic origin are mostly less than +9‰, whereas the metamorphic fluids are usually higher than +3‰ [61]. Therefore, the relatively high and variable $\delta^{18}O_{H2O}$ values of the ore-forming fluids in the quartz separates in the Heihaibei gold deposit are consistent with a metamorphic origin or alternatively a magmatic fluid that was related to the Heihaibei granites hosting the ore, as proposed by [23]. However, we argue that the ore-bearing Heihaibei granites are not the potential source granites because of their initial Pb isotope ratios, which are totally different from the Pb isotopes of ores (see below). Therefore, the ore-forming water is not possibly derived from the magmatic water related to the Heihaibei granites. A deep magmatic water is still possible, but there is no evidence of another granitic intrusion deeper than the Heihaibei granites, and usually, magmatic water that potentially contributes to hydrothermal alteration and corresponding mineralization should be spatio-temporally related to a nearby-granitic intrusion, i.e., the Heihaibei granites. Moreover, the ore-forming fluids in the Heihaibei gold deposit are characterized by low to intermediate salinity, and intermediate to high homogenization temperatures, and no daughter mineral was trapped in the fluid inclusions [23], also lowering the possibilities of magmatic water. Apparently, higher calculated $\delta^{18}O_{H2O}$ values of the fluids are closer to those of most of the orogenic gold deposits suggested by [59]. In a word, we argue a likely metamorphic origin rather than a magmatic water one, although we cannot totally preclude a magmatic origin. The calculated $\delta^{18}O_{H2O}$ values of the Qv1 type of samples (+3.6–+8.3‰, calculated with 340 °C) are commonly higher than those of the Qv2 type of samples (+1.6–+4.3‰, calculated with 240 °C) (Figure 7b), perhaps indicating the mixing of minor meteoric water in the epoch II, because the mixing of metamorphic and meteoric fluids will make the $\delta^{18}O_{H2O}$ values lower. If equilibrium calculations are made at the temperatures indicated by the arsenopyrite geothermometer, both the calculated $\delta^{18}O_{H2O}$ values of the Qv1 type of samples (+5.5–+10.2‰, calculated with 417 °C) and the comparably similar ones of the Qv2 type of samples (+6.6–+9.3‰, calculated with 385 °C) (Figure 7b) are all closer to the field for most orogenic gold deposits suggested by [59], further suggesting a metamorphic origin with relatively high but variable $\delta^{18}O_{H2O}$ values.

Fluid inclusions in 16 quartz separates within the quartz veins at the Heihaibei gold deposit have variable δD values varying from −104.2‰ to −81.1‰ (Table 2), which are apparently lower than those of most orogenic gold deposits suggested by [59], and they are partially plotted in the field of the devolatilization of organic matter in sediments (Figure 7a). However, no report shows organic matter in the sedimentary wall rock in the Heihaibei gold deposit. In some cases, bulk fluids extracted from quartz may be a mixture of primary, pseudosecondary, and secondary inclusions, then low δD values from the bulk extraction of fluid inclusions are often considered to reflect the secondary inclusions formed in the presence of meteoric water during the uplift of the deposits [65–68]. Therefore, we believe that the secondary inclusions formed in the presence of meteoric water during the uplift of the deposits contribute to the depletion of H isotope compositions from the bulk

extraction of fluid inclusions within the quartz in the Heihaibei gold deposit. In this way, the potentially higher δD values may be closer to the δD values of the primary metamorphic ore-forming fluids (Figure 7b). Moreover, low δD values due to the presence of H_2 and/or CH_4 in the aqueous fluid [69] cannot be precluded either; unfortunately, laser Raman spectroscopy has not been carried out. Finally, meteoric water mixing is possible, in order to lower the δD values. Actually, the δD_{VSMOW} values of quartz in the Qv1 type samples are slightly higher (−97.2‰ to −81.1‰) than those of the Qv2 type samples (−104.2‰ to −89.9‰), suggesting mixing with minor meteoric water in epoch II. Overall, both the δD and $\delta^{18}O$ values of the ore-forming fluids showed a slight decrease from epoch I (Qv1 ores) to epoch II (Qv2) (Figure 7b), further indicating mixing with minor meteoric water, especially in epoch II.

The Dazaohuo and Heicigou gold deposits in KLRA have relatively different H and O isotope compositions compared to each other [29], and both are totally different from those of the Heihaibei gold deposit (Figure 7a), suggesting a different source of ore-forming fluids for these gold deposits in the KLHA. However, other gold deposits, i.e., Shenshuitan [4,8–10], Guoluolongwa [19] in the MKL, and Kaihuangbei [14] in the SKL, in which there are both quartz veins and phyllic rock-type ores, have relatively variable H and O isotope compositions relative to gold deposits which have predominant quartz vein ores, such as the Heihaibei gold deposit (this study), as well as the Hongqigou gold deposit [60], perhaps due to higher degrees of water–rock reaction/mixing, and more meteoric water mixing during their mineralization. By the way, the H and O isotope compositions (Figure 7b) for sample K1 are slightly different from other ore samples, perhaps because sample K1 (Qv1 plus Heihaibei granitic wall rock) had experienced a greater extent of water–rock reaction than ore samples in the QV1 or QV2 veins.

5.2. Sulfur Sources

The pyrites from the gold-bearing quartz veins of the Heihaibei gold deposit have almost invariable $\delta^{34}S_{VCDT}$ values ranging from +7.6‰ to +8.7‰, with an average of +8.1‰ (Figure 8a), which span three previously published values of 7.7‰, 7.9‰, and 8.5‰ reported by [23]. Moreover, our sulfur isotopic compositions are within the published $\delta^{34}S$ values for most orogenic gold deposits elsewhere (typically $\delta^{34}S_{VCDT}$ = 0–9‰, [51,67,70,71]). Pyrites from the Qv1 type of samples in the study area have almost invariable $\delta^{34}S$ values ranging from +8.0‰ to +8.7‰ (Figure 8b), which are totally similar to those of pyrites from the Qv2 type samples ranging from +7.6‰ to +8.5 (Figure 8c). As for the large similarities among the sulfides in the Qv1 type samples and those in the Qv2 samples (Figure 8f), as well as the filling mineralization of quartz veins in the Heihaibei gold deposit, we argue that the sulfur in the ores may be derived directly from an ore-forming fluid that had only experienced a temperature decrease and mixing with minor meteoritic water, rather than the apparent sulfur isotope exchange with the wall rock from epoch I to epoch II. The presence of pyrite + arsenopyrite, and the weak alteration assemblage of quartz + sericite in the Heihaibei gold deposit, together with the lack of oxidized phases (hematite) and sulfate minerals, indicate that sulfur was present in the hydrothermal fluids, mainly as reduced sulfur (H_2S) [72,73]. The $\delta^{34}S_{VCDT}$ values for H_2S ($\delta^{34}S_{H2S}$) in equilibrium with sulfides were also estimated by evaluating the $\delta^{34}S_{VCDT}$ values of pyrite using the equilibrium isotopic fractionation factor of sulfide for H_2S suggested by [73], and the average temperature of the hydrothermal fluid during the gold–sulfide mineralization event is inferred as 340 °C for Qv1 (epoch I), and 241 °C for Qv2 (epoch II) (based on the homogenization temperatures reported by [23]). The calculated $\delta^{34}S_{H2S}$ values for H_2S in the hydrothermal fluids ranging from +6.9‰ to +7.6‰, with an average value of +7.08‰ in epoch I, are also very similar to those in the hydrothermal fluids, ranging from +6.1‰ to +7.0‰ in epoch II (Table 3, Figure 8g). Although we did not analyze all types of sulfides in the Heihaibei gold deposit, pyrites dominate the sulfur mass balance, and such an evaluation for the $\delta^{34}S_{H2S}$ values of H_2S in the hydrothermal fluids using the sulfur isotopes of pyrites might be roughly reliable.

Previous researchers have proposed that the relatively high $\delta^{34}S_{VCDT}$ values of the ores were probably derived from the Heihaibei granites [23]. However, if the ore-forming fluids collected and exchanged sulfur from the neighboring Heihaibei granites, the ores in the Heihaibei gold deposit would possibly have more various $\delta^{34}S$ values rather than a narrow range, and different ores would have different $\delta^{34}S$ values because the sulfur isotope ranges of typical granite reservoirs have apparently various $\delta^{34}S$ values and could even range from −13.4‰ to +26.7‰ [74]. Unfortunately, we did not analyze $\delta^{34}S$ values of primary sulfides in the Heihaibei granites, so we are only making a rough guess here. We argue that the relatively high and invariable $\delta^{34}S$ values of sulfides for the Heihaibei gold deposit likely indicate a unique sulfur source directly from deep ore-forming fluids, rather than the neighboring granitic wall rock, because both Qv1 and Qv2 formed directly from primary ore-forming fluids, rather than from the apparent reaction between the ore-forming fluid and the granitic host rock during mineralization. Apparently, prior to upward migration, the deep ore-forming fluids leached sulfur, from the deep source rock in the upper crust, that was homogenized before mineralization.

In the KLHA, compared with the high and invariable $\delta^{34}S$ values of sulfides for the Heihaibei gold deposit, the Dazaohuo gold deposit has more variable $\delta^{34}S$ values of sulfides (Figure 8d, [29]), which are consistent with its phyllic rock-type ores, rather than the quartz veins. As we know, an apparent water–rock reaction which formed phyllic rock-type ores and related hydrothermal alterations possibly resulted in widespread sulfur mixing and exchange, as well as sulfur isotope fractionations in different ores. Therefore, other gold deposits which have predominant phyllic rock-type-ores, i.e., Shenshuitan [4,7,8,15,16], Guoluolongwa [15–17] in the MKL, and Kaihuangbei [20] in the SKL, likely have more variable $\delta^{34}S$ values of sulfides than those in the Heihaibei gold deposit (Figure 8d). Additionally, the Hongqigou gold deposit, which has predominant quartz vein ores, has relatively invariable heavy $\delta^{34}S$ values of sulfides that are similar to this study, indicating an original metamorphic S-bearing fluid [4]. So, once more, the relatively high and invariable $\delta^{34}S$ values of sulfides suggest that the sulfur source is derived directly from a deep metamorphic origin itself, which is consistent with the filling mineralization by the quartz vein, rather than an apparent water–rock reaction.

5.3. Lead Sources

Four pyrite minerals from quartz veins in the Heihaibei gold deposit have relatively invariable Pb isotope compositions (Figure 9a,b). Combined with three previously published sets of Pb isotope ratios ([23] in Figure 9), most of the Pb isotope compositions for sulfides in the Heihaibei gold deposit roughly cluster as a linear group (the blue contour lines in Figure 9a,b), close to the upper crust lead reservoir in the uranogenic plot (Figure 9), which might suggest two-component mixing between a high radiogenic end-member, and another low radiogenic end-member. Apparently, the fields for the Pb isotope compositions of sulfides in the Heihaibei gold deposit are totally different from the fields of the initial Pb isotopes (i.e., the Pb isotopes of K-feldspars) of the Heihaibei granites (the pink dashed lines in Figure 9a,b), and the ores (sulfides) show more radiogenic Pb isotopes and plot roughly along the upper crust growth line (Figure 9), indicating that Au-mineralization was not caused by the Heihaibei granites at ca. 416 Ma. In that way, a granitic intrusion-related gold deposit related to the Heihaibei granites proposed by [23] can be precluded for the Heihaibei gold deposit. Based on the below discussions, we argue that the gold mineralization might have occurred in the Triassic, which was likely around 200 Ma after the formation of the Heihaibei granites that host the veins. The opinion that Pb sources were derived from the neighbor Triassic granites in the north of Fault F51 within the MKL, as shown in Figure 2, might not be a good option, because the Pb isotope compositions of sulfides in the Heihaibei are also apparently different from the Pb isotope compositions of K-feldspars from some Triassic granites in the MKL (e.g., Triassic granites in the Wulonggou area within the MKL reported by [7]). Alternatively, apart from the K-feldspars, the rest of the minerals in the bulk Heihaibei granites will continue to evolve to higher $^{206}Pb/^{204}Pb$, $^{207}Pb/^{204}Pb$,

and $^{208}Pb/^{204}Pb$ due to the U and Th decay for ca. 200 Ma, since they were intruded in the Early Devonian. Using the average U, Th, and Pb abundances of the Heihaibei granite [50] and the possible mineralization age (Triassic, ca. 200 Ma younger than the Early Devonian emplacement), the age (200 Ma)-corrected Pb isotopic ratios, roughly representing the Triassic Pb isotope compositions for the Early Devonian Heihaibei granitic wall rocks, can be estimated (initial Pb isotopes of K-feldspars, plus radiogenic Pb isotopes after ca. 200 Ma decay), and the results show that the age-corrected Triassic Pb isotope groups for the Devonian Heihaibei granites are partially localized within the ore Pb isotope group (Figure 9), indicating that the high radiogenic Pb isotope end-member might be the Triassic Pb isotope group of the Devonian Heihaibei granites. Furthermore, the sulfides within the Sample K1 from [23] have apparently higher radiogenic Pb isotope compositions than other sulfides (Figure 9c,d), perhaps indicating more Pb sources from granitic wall rocks, because Sample K1 was collected in the mineralized granitic wall rock, which would experience more water–rock reactions than the filling ores in QV1 or QV2. Finally, the low radiogenic Pb isotope end-member should be the deep ore-forming fluid itself.

Meanwhile, the Pb isotope compositions of sulfides in the Heihaibei gold deposit are also different from the Dazaohuo gold deposit, which has predominant phyllic rock ores [29] in the KLRA, or other gold deposits in the EKO (Figure 9a,b), also showing they have different Pb sources among them. The variable Pb isotope compositions in the Heihaibei gold deposit have more uranogenic and thorogenic Pb isotope compositions than other gold deposits, which have predominant phyllic rock ores, i.e., Shenshuitan [4,7,9], Guoluolongwa [16,17] in the MKL, and Kaihuangbei [20] in the SKL, also suggesting that Pb sources are distinctive for the Heihaibei gold deposit. Possibly in the Heihaibei gold deposit, the primary ore-forming fluids would have washed through deep parts of the Heihaibei granites with high levels of U/Pb and Th/Pb in the upper crust before final gold mineralization, because the apparent exchanging of the Pb isotopes between the ore-forming fluid and the Heihaibei granitic wall rock is relatively difficult during the gold filling mineralization accompanying the weak water–rock reaction in the Triassic. Pb isotope compositions of sulfides are more variable than sulfur isotopes, likely because the Heihaibei granites commonly contain more variable radiogenic Pb isotopes, which were continuously increased from U and Th decay than from sulfur stable isotopes. Moreover, the Qv1 type of ore has slightly more uranogenic and thorogenic Pb isotopes than the Qv2 type (Figure 9c,d), likely indicating less of a mixing of the Triassic Pb source of the Heihaibei granites in epoch II than epoch I, because the low-temperature ore-forming fluid of the epoch II might have experienced less Pb isotope exchanging with the deep parts of the Heihaibei granites or the upper crust before gold mineralization.

5.4. Genetic Type and Possible Metallogenic Model

Genetic classification of the Heihaibei gold deposit remains controversial: a hydrothermal-vein-type gold deposit [22], a magmatic hydrothermal gold deposit [24], an orogenic gold deposit [25], or a granitic intrusion-related gold deposit related to the Heihaibei granites [23] have all been proposed. However, as mentioned above, the ore bodies in the Heihaibei gold deposit are usually delineated in quartz veins along subsidiary faults within the Heihaibei granites, and the Heihaibei granites (monzogranites and granodiorites) are wall rocks for gold mineralization. Furthermore, many of the geological and geochemical features of the Heihaibei gold deposit are similar to those of the orogenic gold deposits, as described by [51]. These features include: (1) the geodynamic setting of the Heihaibei gold deposit related with the Triassic evolution of the EKO; (2) the gold mineralization controlled and hosted by the subsidiary faults of Fault F51 (a segment of the M. KLF) within the Heihaibei area, as well as in the KLRA; (3) the major sulfide minerals (contents < 5%) represented by pyrite and arsenopyrite, with minor chalcopyrite, galena, sphalerite, tetrahedrite, and micro-native gold; (4) the weak alteration assemblage, including silicification, and sericitization, with minor chloritization and carbonatization, similar to some typical orogenic gold deposits; (5) the major ore-forming fluids showing H_2O-NaCl fluids with

low salinity (3.69~16.63 equiv. wt% NaCl), and intermediate to high homogenization temperatures from 183 to 412 °C [23]; (7) the δD values (−104.2 to −81.1‰) and estimated $\delta^{18}O$ values (+1.6 to +8.3‰, or even from +5.5 to +10.2‰) for ore-forming fluids, indicating a metamorphic water rather than a magmatic water; (8) the $\delta^{34}S$ values of sulfides from +7.6‰ to +8.7‰, suggesting a sulfur source that is directly from the deep ore-forming fluids themselves, with sulfur isotope homogenization; and (9) the Pb isotopic compositions of sulfides, with $^{206}Pb/^{204}Pb$ ratios of 18.7219–19.0007, $^{207}Pb/^{204}Pb$ ratios of 15.6959–15.7062, and $^{208}Pb/^{204}Pb$ ratios of 37.7359–38.8055, showing partial similarities to the age-corrected Triassic Pb isotope compositions of the Devonian Heihaibei granitic wall rocks, rather than to the initial Pb isotope compositions of the granite at its time of emplacement 416 Ma ago, indicating a mixed Pb source between the deep ore-forming fluids and the Triassic Pb isotope compositions of the deep Devonian Heihaibei granitic wall rock, and some affinities to upper crust lead reservoirs [62]. Based on the results described above, and the comparison with typical orogenic gold deposits, we propose that the Heihaibei gold deposit belongs to the orogenic gold category, as described by [51], rather than a granitic intrusion-related gold deposit proposed by [23].

To date, mineralization in the Heihaibei gold deposit, whose timing has not been determined directly by radiometric dating but must be later than the Early Devonian (416 Ma, [50]) of the monzogranite wall rocks. As mentioned above, the EKO has undergone at least two orogenies that are closely related to the consumption of the Neo-Proterozoic to Early Devonian Proto-Tethys Ocean, which lays along the M.KLF, and the Carboniferous to Late Triassic Paleo-Tethys Ocean, which lays along the S.KLF–AMF, respectively [3,31,37]. We have previously considered that the EKO during the Late Early Silurian–Middle Devonian (430–389 Ma) was in the post-collisional stage related to the closure of the Proto-Tethys Ocean [75], and that the A-type Heihaibei granites were exact products of post-collisional magmatic emplacement during the post-collisional stage [50]. The northward subduction of the Paleo-Tethys oceanic plate was not initiated until the Carboniferous [3,31,37]. From the Middle Devonian (389 Ma) to the Carboniferous, the tectonism and magmatism in the EKO would have been relatively rare, as well as the gold mineralization here. Actually, numerous magmatic emplacements which are related to the evolution (the subduction and subsequent collision) of the Paleo-Tethys Ocean between the SKL and BH–SG happened predominantly from the Late Permian to the Triassic [42,44,46,75,76]. Additionally, it was in the Early to Middle Triassic that the EKO was strongly affected by the northward subduction of the Paleo-Tethys oceanic plate, and it was in the Late Triassic that the EKO was dominated by the closure of the Paleo-Tethys oceans between the EKO and BH–SG [46]. Accompanying the Early to Middle Triassic subduction and the Late Triassic collision, most typical gold deposits within the EKO have predominant Triassic mineralization ages varying from 237 Ma to <215 Ma, e.g., Shenshuitan (zircon U-Pb dating, <215 Ma, [13]; sericite Ar-Ar dating, 237.0 Ma and 230.8 Ma, [8]), Shihuigou (sericite Ar-Ar dating, 236.5 Ma, [77]; zircon fission track thermochronology, 235–216 Ma [12]), Hongqigou (zircon fission track thermochronology, 223 Ma, [12]), Guoluolongwa (sericite Ar-Ar dating, 202.7 Ma for the late stage of mineralization [78]; and Re-Os dating, 375 Ma and 354 Ma for the early stage of mineralization [18]). With this in mind, we consider that a Triassic age of gold mineralization in the Heihaibei gold deposit may be reasonable.

We previously argued that the ancient metamorphic fluid, perhaps produced during the Precambrian metamorphism in the EKO, cannot explain the predominant Triassic orogenic gold mineralization found in the Wulonggou area in the EKO [4]. Even in the Late Triassic, the soft collision between EKO and BH–SG [33] cannot produce metamorphism of the deep rocks and subsequent metamorphic fluids at depth in the lower crust [4]. If this is the case, the slab devolatilization model proposed for the Jiaodong gold province [79] may be also applicable to the Heihaibei gold deposit, as with the Shenshuitan gold deposit (e.g., [4]). In their model, the late-orogenic metamorphic devolatilization of stalled subduction slabs and oceanic sediments may directly produce metamorphic fluids, and the overpressured slab-derived metamorphic fluids might also be channeled directly into

crustal-scale faults with subsequent upward flow [63,79]. Based on the above discussion, the Heihaibei gold deposit may be associated with the subduction of the Paleo-Tethys oceanic plate in the Early to Middle Triassic, or even the collision between BH–SG and EKO in the Later Triassic. Therefore, during the Triassic in the EKO, the slab-derived metamorphic fluids may be initiated following the EKO Triassic geodynamic evolution, and they might have migrated through the first-order crustal-scale faults (i.e., M.KLF) upward into the subsidiary faults at higher levels (i.e., Fault F53) (Figure 10). During the migration of these deep slab-derived metamorphic fluids, sulfur, lead, and gold may be leached from various types of surrounding source rocks in the upper crust. According to the highly radiogenic Pb isotope ratios in this study, we likely infer that such slab-derived fluids may wash up high U/Pb and Th/Pb source rock, i.e., the deep part of the Heihaibei granites, in the upper crust, before upward gold mineralization; then, such slab-derived fluid actually becomes a special ore-forming fluid, since it migrates across such a "strongly leached zone" in the upper crust (Figure 10). Eventually, in the Heihaibei gold deposit, such evolved slab-derived metamorphic water with leached ore-forming materials (such as gold, sulfur, arsenic, iron, lead, copper, zinc, etc.) may continue to migrate upward, become a special ore-forming metamorphic fluid, and periodically deposit quartz veins within shallow subsidiary faults, likely because of a sudden change of physico-chemical conditions rather than strong water–rock reactions between ore-forming fluids and wall rocks. A similar filling mineralization of quartz veins in subsidiary faults could be found in other gold deposits, such as the Heicigou gold deposit [29] in the KLRA, and the Hongqigou gold deposit [18] in the MKL, etc. During the predominant filling of quartz veins in subsidiary faults in the Heihaibei gold deposit, minor water–rock interactions may also occur in the granitic wall rocks and contribute to weak hydrothermal alterations within brecciated granitic wall rocks, minor ores of stockwork quartz veinlets, or breccias in such altered granites. The late stage of tectonic movements due to the soft collision between EKO and BH–SG may deform previously formed quartz veins (Qv1 and Qv2) along fault belts in the Heihaibei gold deposit and form breccia ores, indicating that the deformation stage occurred. Given that there is a strong water–rock interaction between the ore-forming metamorphic water and wall rocks, important phyllic-type ores and strong hydrothermal alterations would have occurred, such as in other gold deposits, e.g., Dazaohuo [29], and the Shenshuitan gold deposit in the Wulonggou gold field [4,7–10]. Certainly, both the filling of quartz veins and phyllic rocks could be found simultaneously in certain other gold deposits in the EKO, such as the Guoluolongwa gold deposit [14–19] and the Kaihuangbei gold deposit [14,20], mostly because of various characteristics of the ore-forming faults.

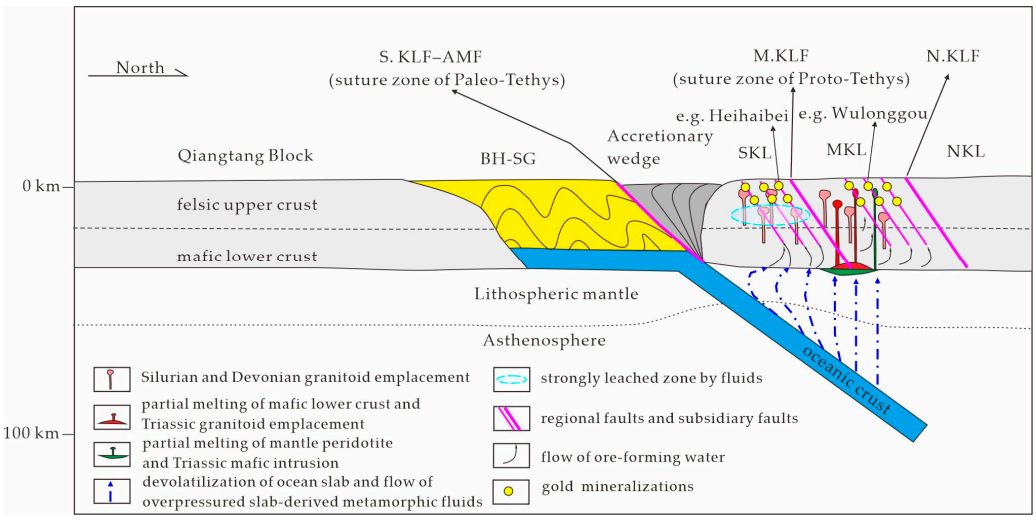


Figure 10. Metallogenic model for the Heihaibei gold deposit, as well as gold deposits in the EKO. Abbreviations are the same as those in Figure 1.

6. Conclusions

From the H, O, S, and Pb isotope compositions of ores from the Heihaibei gold deposit in the KLRA reported in this study the following conclusions can be derived.

The measured $\delta^{18}O_{quartz}$ values for the quartz from the auriferous quartz veins in the Heihaibei gold deposit range from +9.2‰ to +13.9‰, and the estimated $\delta^{18}O$ values for ore-forming fluids range from +1.6‰ to +8.3 ‰, or even up to +5.5 to +10.2‰. The δD_{H2O} values for the fluid inclusions of the quartz range from -104.2‰ to -81.1‰. The results suggest that the ore-forming fluid is a special metamorphic water, perhaps somewhat modified by interaction with meteoric waters.

The $\delta^{34}S$ values of sulfide separates from auriferous quartz veins in the Heihaibei gold deposit range from +7.6‰ to +8.7‰, and the calculated $\delta^{34}S_{H2S}$ values for H_2S in the ore-forming fluids range from +6.1‰ to +7.6‰, suggesting that the sulfur sources may be directly derived from the deep ore-forming fluids themselves.

Six potassic feldspar separates from the Heihaibei granites have apparently invariable Pb isotope compositions, with $^{206}Pb/^{204}Pb$ ratios of 18.3532 to 19.4864, $^{207}Pb/^{204}Pb$ ratios of 15.6475 to 15.6812, and $^{208}Pb/^{204}Pb$ ratios of 37.1750 to 38.4598. Additionally, the Pb isotope compositions of sulfide separates from the auriferous quartz veins in the Heihaibei gold deposit range, from 118.7219 to 19.0007 for $^{206}Pb/^{204}Pb$, 15.6959 to 15.7062 for $^{207}Pb/^{204}Pb$, and 37.7359 to 38.8055 for $^{208}Pb/^{204}Pb$, showing partial similarities to the age (200 Ma)-corrected Triassic Pb isotope compositions of the Devonian Heihaibei granitic wall rocks, rather than the initial Pb isotope compositions of the granites, indicating a mixed Pb source between the deep ore-forming fluids and the Triassic Pb isotope compositions of the deep parts of the Devonian Heihaibei, and showing some affinities to the upper crust lead reservoir.

The Heihaibei gold deposit may be classified as an orogenic gold deposit, which is associated with the subduction of the Paleo-Tethys oceanic plate in the Early to Middle Triassic, or even the collision between BH–SG and EKO in the Later Triassic. The slab-derived metamorphic fluids may be generated during the above Triassic geodynamic evolution and subsequently leached ore-forming materials from high U/Pb and Th/Pb source rock, i.e., the deep parts of the Heihaibei granites and their comagmatic granitoids in the upper crust. Then, they continuously migrated upward to the subsidiary faults in the KLRA or even the whole EKO, mixed with minor meteoric water, especially during the later epoch of gold mineralization, and periodically deposited quartz veins within shallower subsidiary faults in the Heihaibei gold deposit. Late stages of tectonic movements may deform previously formed quartz veins along fault belts and form breccia ores.

Supplementary Materials: The following are available online at https://www.mdpi.com/article/10.3390/min13020274/s1, Table S1: H and O isotope data for quartz in the Heihaibei gold deposit; Table S2: Sulfur isotope data for sulfides in the Heihaibei deposit; Table S3: Pb isotope compositions for sulfides in the Heihaibei gold deposit.

Author Contributions: Author Contributions: Conceptualization, Q.-F.D.; methodology, H.J., X.Z. and R.-Z.W.; software, X.Z. and R.-Z.W.; validation, H.-F.L., Q.-F.D., R.-Z.W. and T.P.; formal analysis, H.-F.L., X.Z., R.-Z.W. and Q.-F.D.; investigation, H.-F.L., H.J., R.-Z.W., X.Z. and Q.-F.D.; resources, H.-F.L., T.P., H.J. and Q.-F.D.; data curation, H.-F.L. and Q.-F.D.; writing—original draft preparation, H.-F.L. and Q.-F.D.; writing—review and editing, H.-F.L. and Q.-F.D.; visualization, H.-F.L., X.Z. and Q.-F.D.; supervision, T.P. and Q.-F.D.; project administration, H.-F.L. and Q.-F.D.; funding acquisition, H.-F.L. and Q.-F.D. All authors have read and agreed to the published version of the manuscript.

Funding: This research was funded by the Action Plan of Kunlun Talents, Qinghai Talent Office file (2020) No. 18.

Institutional Review Board Statement: Not applicable.

Informed Consent Statement: Not applicable.

Data Availability Statement: The datasets generated during and/or analyzed during the current study are available in full within the published article and its supplementary materials.

Acknowledgments: We are grateful to the analytical Laboratories at CAGS and BCTT for their help with the stable isotope analyses.

Conflicts of Interest: The authors declare no conflict of interest.

References

1. Bian, Q.T.; Li, D.H.; Pospelov, I.; Yin, L.M.; Li, H.S.; Zhao, D.S.; Chang, C.F.; Luo, X.Q.; Gao, S.L.; Astrakhantsev, O.; et al. Age, geochemistry and tectonic setting of Buqingshan ophiolites, North Qinghai–Tibet Plateau, China. *J. Asian Earth Sci.* **2004**, *23*, 577–596. [CrossRef]
2. Xu, Z.Q.; Yang, J.S.; Li, H.B.; Zhang, J.X.; Wu, C.L. *Terrane Amalgamation, Collision and Uplift in the Qinghai–Tibet Plateau*; Geological Publishing House: Beijing, China, 2007; p. 458.
3. Jiang, C.F.; Yang, J.S.; Feng, B.G.; Zhu, Z.X.; Zhao, M.; Chai, Y.C.; Shi, X.D.; Wang, H.D. *Opening Closing Tectonics of Kunlun Shan*; Geological Publishing House: Beijing, China, 1992; p. 217.
4. Zhou, X.; Pan, T.; Ding, Q.-F.; Cheng, L.; Song, K.; Liu, F.; Gao, Y. Isotope Geochemistry of the Shenshuitan Gold Deposit within the Wulonggou Gold Field in the Eastern Kunlun Orogen, Northwest China: Implications for Metallogeny. *Minerals* **2022**, *12*, 339. [CrossRef]
5. Li, Z.M.; Xue, C.J.; Wang, X.H.; Tang, H.; Tu, Q.J.; Teng, J.X.; Li, R.S. Features of regional mineralization and analysis of the exploration development in the Eastern Kunlun Mountains. *Geol. Rev.* **2007**, *53*, 708–718, (In Chinese with English abstract).
6. Du, Y.L.; Jia, Q.Z.; Han, S.F. Mesozoic tectono-magmatic-mineralization and copper-gold polymetallic ore prospecting research in East Kunlun Metallogenic Belt in Qinghai. *Northwestern Geol.* **2012**, *45*, 69–75, (In Chinese with English abstract). [CrossRef]
7. Liu, F. Research on the Geological, Geochemical Characteristics and Genesis of Shenshuitan Gold Deposit in the Wulonggou Ore Concentration District in the Eastern Kunlun Orogenic Belt, Qinghai Province. Master's Thesis, Jilin University, Changchun, China, 2017.
8. Zhang, J.Y.; Ma, C.Q.; Li, J.W.; Pan, Y.M. A possible genetic relationship between orogenic gold mineralization and post-collisional magmatism in the eastern Kunlun Orogen, western China. *Ore Geol. Rev.* **2017**, *81*, 342–357. [CrossRef]
9. Zhang, Y.T. Research on Metallogenesis of Gold Deposits in the Wulongou Ore Concentration Area, Central Segment of the East Kunlun Mountains, Qinghai Province. Ph.D. Thesis, Jilin University, Changchun, China, 2018.
10. Song, K. Research on the Metallogenic Geological Background and Genesis of Huanglonggou Ore Block in Shenshuitan Gold Deposit in the Wulonggou Ore Concentration Area in the Eastern Kunlun Orogenic Belt, Qinghai Province. Master's Thesis, Jilin University, Changchun, China, 2019.
11. Tian, C.S. Research on Gold Mineralization and Metallogenic Prognosis of Wulonggou Goldfield in the Eastern Kunlun Orogen. Ph.D. Thesis, China University of Geosciences, Beijing, China, 2012.
12. Yuan, W.M.; Mo, X.X.; Zhang, A.K.; Chen, X.N.; Duan, H.W.; Li, X.; Hao, N.N.; Wang, X.M. Fission Track thermochronology evidence for multiple periods of mineralization in the Wulonggou Gold Deposits, Eastern Kunlun Mountains, Qinghai province. *J. Earth Sci.* **2013**, *24*, 471–478. [CrossRef]
13. Ding, Q.F.; Jiang, S.Y.; Sun, F.Y. Zircon U–Pb geochronology, geochemical and Sr–Nd–Hf isotopic compositions of the Triassic granite and diorite dikes from the Wulonggou mining area in the Eastern Kunlun Orogen, NW China: Petrogenesis and tectonic implications. *Lithos* **2014**, *205*, 266–283. [CrossRef]
14. Feng, C.Y.; Zhang, D.Q.; Wang, F.C.; Li, D.X.; She, H.Q. Geochemical characteristics of ore-forming fluids from the orogenic Au (and Sb) deposits in the eastern Kunlun area, Qinghai province. *Acta Petro Sin.* **2004**, *20*, 949–960, (In Chinese with English abstract). [CrossRef]
15. Chen, J.J. Paleozoic-Mesozoic Tectono-Magmatic Evolution and Gold Mineralization in Gouli Area, East End of East Kunlun Orogen. Ph.D. Thesis, China University of Geosciences, Wuhan, China, 2018.
16. Hu, R.G. Research on Geological-Geochemial Characteristics and Genesis of the Guoluolongwa Gold Deposit in Qinghai Province. Master's Thesis, Central South University, Changsha, China, 2008.
17. Yue, W.H. Study on Metallogenic Mechanism and Geological-Geochemical Characteristics of Typical Deposits in Gouli Gold Ore Concentration Area in the Eastern Segment of the Eastern Kunlun Orogen. Ph.D. Thesis, Kunming University of Science and Technology, Kunming, China, 2013.
18. Chen, J.; Fu, L.; Selby, D.; Wei, J.; Zhao, X.; Zhou, H. Multiple episodes of gold mineralization in the East Kunlun Orogen, western Central Orogenic Belt, China: Constraints from Re-Os sulfide geochronology. *Ore Geol. Rev.* **2020**, *123*, 103587. [CrossRef]
19. Ding, Q.F.; Jin, S.K.; Wang, G.; Zhang, B.L. Ore-forming fluid of the Guoluolongwa gold deposit in Dulan County, Qinghai province. *J. Jilin Univ. Earth Sci. Ed.* **2013**, *42*, 415–426, (In Chinese with English abstract).
20. Feng, C.Y.; Zhang, D.Q.; Li, D.X.; She, H.Q. Sulfur and lead isotope geochemistry of the orogenic gold deposits in East Kunlun area, Qinghai province. *Acta Geosci. Sin.* **2003**, *24*, 593–598, (In Chinese with English abstract). [CrossRef]
21. Wang, Q.Y.; Dong, Y.J.; Pan, Y.M.; Liao, F.X.; Guo, X.W. Early Paleozoic Granulite-Facies Metamorphism and Magmatism in the Northern Wulan Terrane of the Quanji Massif: Implications for the Evolution of the Proto-Tethys Ocean in Northwestern China. *J. Earth Sci.* **2018**, *29*, 1081–1101. [CrossRef]
22. QIGEIQP. *Report of Detailed Exploration for Heihaibei Gold Deposit in Golmud City, Qinghai Province*; Qaidam Integrated Geological Exploration Institute of Qinghai Province (QIGEIQP): Golmud, China, 2021; pp. 1–328, (In Chinese with English abstract).

23. Yu, L.; Sun, F.; Beier, C.; Wu, D.; Li, L.; Wang, L.; Huang, G.; Fan, X.; Xu, C. Geology, U-Pb geochronology and stable isotope geochemistry of the Heihaibei gold deposit in the southern part of the Eastern Kunlun Orogenic Belt, China: A granitic intrusion-related gold deposit? *Ore Geol. Rev.* **2022**, *144*, 104859. [CrossRef]
24. Huang, G.; Ma, W.; Li, C.; Jiao, H. Geological characteristics and prospecting prospects of Heihaibei gold deposit in Kunlunhe area, Qinghai province. *Gold* **2021**, *42*, 26–30, (In Chinese with English abstract).
25. Jiao, H.; Kang, J.Z.; Huang, G.B.; Jia, J.T.; Peng, J. Magmatism, metallogenic characteristics, and prospecting prediction for gold deposits in the north of Kunlun River area, Qinghai, China. *J. Geomech.* **2022**, *28*, 383–405, (In Chinese with English abstract). [CrossRef]
26. Han, G. A Study on the Geological Characteristics of Gold Mineralization in Heihaibei Region, East Kunlun, Qinghai Province. Master's Thesis, China University of Geosciences, Beijing, China, 2013.
27. Li, J. Metallogenic Regularity and Metallogenic Prognosis of Gold Deposit in the East Kunlun Orogen, Qinghai Province. Ph.D. Thesis, Chang'an University, Xi'an, China, 2017.
28. Shen, H. Geochemical Characteristics and Ore Genesis of the Heihainan Gold Deposit in the Kunlun River District, Qinghai Province. Master's Thesis, China University of Geosciences, Beijing, China, 2016.
29. Feng, L. Geological and Geochemical Characteristics and Ore Genesis of the Gold Deposits in the Kunlun River District, Qinghai Province. Master's Thesis, China University of Geosciences, Beijing, China, 2017.
30. An, H.; Han, G.; Wu, P.; Wu, M.; Han, W. Deposit geological characteristics and prospecting potential of Dazaohuogou-Heicigou gold mine in Qinghai province. *Metal Mine* **2018**, *9*, 127–136, (In Chinese with English abstract).
31. Yang, J.S.; Robinson, P.T.; Jiang, C.F.; Xu, Z.Q. Ophiolites of the Kunlun Mountains, China and their tectonic implications. *Tectonophysics* **1996**, *258*, 215–231. [CrossRef]
32. Pan, Y.S.; Zhou, W.M.; Xu, R.H.; Wang, D.A.; Zhang, Y.Q.; Xie, Y.W.; Chen, T.E.; Luo, H. Geological characteristics and evolution of the Kunlun Mountains region during the early Paleozoic. *Sci. China Ser. D* **1996**, *39*, 337–347.
33. Yin, A.; Harrison, T.M. Geologic evolution of the Himalayan-Tibetan orogen. *Annu. Rev. Earth Planet. Sci.* **2000**, *28*, 211–280. [CrossRef]
34. Roger, F.; Arnaud, N.; Gilder, S.; Tapponnier, P.; Jolivet, M.; Brunel, M.; Malavieille, J.; Xu, Z.Q.; Yang, J.S. Geochronological and geochemical constraints on Mesozoic suturing in east central Tibet. *Tectonics* **2003**, *22*, 1037. [CrossRef]
35. Harrowfield, M.J.; Wilson, C.J.L. Indosinian deformation of the Songpan Garze Fold Belt, northeast Tibetan Plateau. *J. Struct. Geol.* **2005**, *27*, 101–117. [CrossRef]
36. Reid, A.J.; Wilson, C.J.L.; Liu, S. Structural evidence for the Permo-Triassic tectonic evolution of the Yidun Arc, eastern Tibetan plateau. *J. Struct. Geol.* **2005**, *27*, 119–137. [CrossRef]
37. Yang, J.S.; Shi, R.D.; Wu, C.L.; Wang, X.B.; Robinson, P.T. Dur'ngoi Ophiolite in East Kunlun, Northeast Tibetan Plateau: Evidence for Paleo-Tethyan Suture in Northwest China. *J. Earth Sci.* **2009**, *20*, 303–331. [CrossRef]
38. Pan, G.T.; Ding, J.; Wang, L.; Zhuang, Y.; Wang, Q.; Zhai, G.; Wang, D. Important new progress in regional geological survey of Qinghai Tibetan Plateau. *Geol. Bull. China* **2002**, *21*, 787–793, (In Chinese with English abstract).
39. Liu, Y.J.; Genser, J.; Neubauer, F.; Jin, W.; Ge, X.H.; Handler, R.; Takasu, A. Ar-40/Ar-39 mineral ages from basement rocks in the Eastern Kunlun Mountains, NW China, and their tectonic implications. *Tectonophysics* **2005**, *398*, 199–224. [CrossRef]
40. Gao, Y.; Li, W.; Li, Z.; Wang, J.; Hattori, K.; Zhang, Z.; Geng, J. Geology, geochemistry, and genesis of Tungsten-Tin deposits in the Baiganhu district, Northern Kunlun Belt, Northwestern China. *Econ. Geol.* **2014**, *109*, 1787–1799. [CrossRef]
41. Meng, F.C.; Cui, M.H.; Wu, X.K.; Ren, Y.F. Heishan mafic-ultramafic rocks in the Qimantag area of Eastern Kunlun, NW China: Remnants of an early Paleozoic incipient island arc. *Gondwana Res.* **2015**, *27*, 745–759. [CrossRef]
42. Liu, C.D.; Mo, X.X.; Luo, Z.H.; Yu, X.H.; Chen, H.W.; Li, S.W.; Zhao, X. Mixing events between the crust- and mantle-derived magmas in Eastern Kunlun: Evidence from zircon SHRIMP II chronology. *Chin. Sci. Bull.* **2004**, *49*, 828–834. [CrossRef]
43. Yuan, C.; Sun, M.; Xiao, W.; Wilde, S.; Li, X.; Liu, X.; Long, X.; Xia, X.; Ye, K.; Li, J. Garnet-bearing tonalitic porphyry from East Kunlun, Northeast Tibetan Plateau: Implications for adakite and magmas from the MASH Zone. *Int. J. Earth Sci.* **2009**, *98*, 1489–1510. [CrossRef]
44. Zhang, J.Y.; Ma, C.Q.; Xiong, F.H.; Liu, B. Petrogenesis and tectonic significance of the Late Permian-Middle Triassic calc-alkaline granites in the Balong region, eastern Kunlun Orogen, China. *Geol. Mag.* **2012**, *149*, 892–908. [CrossRef]
45. Huang, H.; Niu, Y.L.; Nowell, G.; Zhao, Z.D.; Yu, X.H.; Zhu, D.C.; Mo, X.X.; Ding, S. Geochemical constraints on the petrogenesis of granitoids in the East Kunlun Orogenic belt, northern Tibetan Plateau: Implications for continental crust growth through syn-collisional felsic magmatism. *Chem. Geol.* **2014**, *370*, 1–18. [CrossRef]
46. Ding, Q.F.; Liu, F.; Yan, W. Zircon U–Pb geochronology and Hf isotopic constraints on the petrogenesis of Early Triassic granites in the Wulonggou area of the Eastern Kunlun Orogen, Northwest China. *Int. Geol. Rev.* **2015**, *57*, 1735–1754. [CrossRef]
47. Chen, N.; Sun, M.; Wang, O.; Zhao, G.; Chen, Q.; Shu, G. EMP chemical ages of monazites from Central Zone of the eastern Kunlun Orogen: Records of multi-tectonometamorphic events. *Chin. Sci. Bull.* **2007**, *52*, 2252–2263. [CrossRef]
48. Xin, W.; Sun, F.Y.; Li, L.; Yan, J.M.; Zhang, Y.T.; Wang, Y.C.; Shen, T.S.; Yang, Y.J. The Wulonggou metaluminous A2-type granites in the Eastern Kunlun Orogenic Belt, NW China: Rejuvenation of subduction-related felsic crust and implications for post-collision extension. *Lithos* **2018**, *312–313*, 108–127. [CrossRef]

49. Gu, X.X.; Zhang, Y.M.; Feng, L.Q.; He, G.; Wang, J.L.; Kang, J.Z.; Wang, B.Z. Recognition, age determination and tectonic significance of the Kunlun River ductile shear zone in the East Kunlun Mountains. *Geol. Bull. China* **2018**, *37*, 345–355, (In Chinese with English abstract).
50. Lu, H.L.; Pan, T.; Jiao, H.; Ding, Q.F.; Zheng, T.; Zhou, X.; Wu, R. Geochronology, geochemistry, and Hf isotopic compositions of the Early Devonian Heihaibei granite in the East Kunlun Orogen, Northwest China. *Can. J. Earth Sci.* **2022**, *59*, 566–579. [CrossRef]
51. Groves, D.I.; Goldfarb, R.J.; Gebre-Mariam, M.; Hagemann, S.G.; Robert, F. Orogenic gold deposits: A proposed classification in the context of their crustal distribution and relationship to other gold deposit types. *Ore Geol. Rev.* **1998**, *13*, 7–27. [CrossRef]
52. Clayton, R.N.; O'Neil, J.R.; Mayeda, T.K. Oxygen isotope exchange between quartz and water. *J. Geophys. Res.* **1972**, *77*, 3057–3067. [CrossRef]
53. Clayton, R.N.; Mayeda, T.K. The use of bromine pentafluoride in the extraction of oxygen from oxides and silicates for isotopic analysis. *Geochim. Cosmochim. Acta* **1963**, *27*, 43–52. [CrossRef]
54. Ding, Q.F.; Jiang, S.Y.; Sun, F.Y.; Qian, Y.; Wang, G. Origin of the Dachang gold deposit, NW China: Constraints from H, O, S, and Pb isotope data. *Int. Geol. Rev.* **2013**, *55*, 1885–1901. [CrossRef]
55. Gong, B.; Zheng, Y.F.; Chen, R.X. An online method combining a thermal conversion elemental analyzer with isotope ratio mass spectrometry for the determination of hydrogen isotope composition and water concentration in geological samples. *Rapid Commun. Mass Spectrom.* **2007**, *21*, 1386–1392. [CrossRef] [PubMed]
56. Robinson, B.W.; Kusakabe, M. Quantitative preparation of sulfur dioxide, for sulfur-34/sulfur-32 analyses, from sulfides by combustion with cuprous oxide. *Anal. Chem.* **1975**, *47*, 1179–1181. [CrossRef]
57. He, Z.; Zhang, X.; Deng, X.; Hu, H.; Li, Y.; Yu, H.; Archer, C.; Li, J.; Huang, F. The behavior of Fe and S isotopes in porphyry copper systems: Constraints from the Tongshankou Cu-Mo deposit, Eastern China. *Geochim. Cosmochim. Acta* **2020**, *270*, 61–83. [CrossRef]
58. Chen, D.; Han, Y.; Wang, Z.; Chen, K.; Cai, B.; Liu, S. The prestigious tin–lead horse fittings in the Warring States Period: Evidence from funerary artefacts of a Warring States Tomb at Shouxian, Anhui. *Archaeometry* **2021**, *63*, 1290–1305. [CrossRef]
59. Goldfarb, R.J.; Ayuso, R.; Miller, M.L.; Ebert, S.W.; Marsh, E.E.; Petsel, S.A.; Miller, L.D.; Bradley, D.; Johnson, C.; McClelland, W. The Late Cretaceous Donlin Creek gold deposit, southwestern Alaska: Controls on epizonal ore formation. *Econ. Geol.* **2004**, *99*, 643–671. [CrossRef]
60. Cheng, L. Study on the Geological and Geochemical Characteristics and Genesis of Hongqigou Gold Deposit, Wulonggou Ore Concentration Area, East Kunlun, Qinghai Province. Master's Thesis, Jilin University, Changchun, China, 2020.
61. Sheppard, S. Characterization and isotopic variations in natural waters. *Rev. Mineral. Geochem.* **1986**, *16*, 165–183.
62. Zartman, R.E.; Doe, B.R. Plumbotectonics—The model. *Tectonophysics* **1981**, *75*, 135–162. [CrossRef]
63. Goldfarb, R.J.; Groves, D.I. Orogenic gold: Common or evolving fluid and metal sources through time. *Lithos* **2015**, *233*, 2–26. [CrossRef]
64. Bierlein, F.P.; Crowe, D.E. Phanerozoic orogenic lode gold deposits. In *Gold in 2000. Reviews in Economic Geology*; Hagemann, S.G., Brown, P.E., Eds.; Society of Economic Geologists, Inc.: Littleton, CO, USA, 2000; Volume 13, pp. 103–139.
65. Pickthorn, W.J.; Goldfarb, R.J.; Leach, D.L. Comment and Reply on "Dual origins of lode gold deposits in the Canadian Cordillera": COMMENT. *Geology* **1987**, *15*, 471–472. [CrossRef]
66. Goldfarb, R.J.; Snee, L.W.; Miller, L.D.; Newberry, R.J. Rapid dewatering of the crust deduced from ages of mesothermal gold deposits. *Nature* **1991**, *354*, 296–298. [CrossRef]
67. McCuaig, T.C.; Kerrich, R. P–T–t-deformation-fluid characteristics of lode gold deposits: Evidence from alteration systematics. *Ore Geol. Rev.* **1998**, *12*, 381–453. [CrossRef]
68. Jiang, S.H.; Nie, F.J.; Hu, P.; Lai, X.R.; Liu, Y.F. Mayum: An orogenic gold deposit in Tibet, China. *Ore Geol. Rev.* **2009**, *36*, 160–173. [CrossRef]
69. Fyon, J.A.; Crocket, J.H.; Schwartz, H.P. The Carshaw and Malga Iron-Formation Hosted Gold Deposits of the Timmins Area. In *The Geology of Gold in Ontario*; Colvine, A.C., Ed.; Ontario Geological Survey: Sudbury, ON, Canada, 1984; pp. 98–110.
70. Kerrich, R.; Goldfarb, R.; Groves, D.; Garwin, S.; Jia, Y. The characteristics, origins, and geodynamic settings of supergiant gold metallogenic provinces. *Sci. China Ser. D* **2000**, *43*, 1–68. [CrossRef]
71. Goldfarb, R.J.; Groves, D.I.; Gardoll, S. Orogenic gold and geologic time: A global synthesis. *Ore Geol. Rev.* **2001**, *18*, 1–75. [CrossRef]
72. Ohmoto, H.; Rye, R.O. Isotopes of Sulfur and Carbon. In *Geochemistry of Hydrothermal Ore Deposits*, 2nd ed.; Barnes, H.L., Ed.; John Wiley: New York, NY, USA, 1979; pp. 509–567.
73. Ohmoto, H.; Goldhaber, M.B. Sulfur and carbon Isotopes. In *Geochemistry of Hydrothermal Ore Deposits*, 3rd ed.; Barnes, H.L., Ed.; John Wiley: New York, NY, USA, 1997; pp. 517–611.
74. Zheng, Y.F.; Chen, J.F. *Stable Isotope Geochemistry*; Science Press: Beijing, China, 2000; p. 316.
75. Ding, Q.F.; Song, K.; Zhang, Q.; Yan, W.; Liu, F. Zircon U–Pb geochronology and Hf isotopic constraints on the petrogenesis of the Late Silurian Shidonggou granite from the Wulonggou area in the Eastern Kunlun Orogen, Northwest China. *Int. Geol. Rev.* **2019**, *61*, 1666–1689. [CrossRef]
76. Mo, X.X.; Luo, Z.H.; Deng, J.F.; Yu, X.H.; Liu, C.D.; Chen, H.W.; Yuan, W.M.; Liu, Y.H. Granitic intrusions and crustal growth in the East-Kunlun orogenic belt. *Geol. J. China Univ.* **2007**, *13*, 403–414, (In Chinese with English abstract). [CrossRef]

77. Zhang, D.Q.; Dang, X.Y.; She, H.Q.; Li, D.X.; Feng, C.Y.; Li, J.W. Ar–Ar dating of orogenic gold deposits in the northern margin of Qaidam and East Kunlun Mountains and its geological significance. *Miner. Depos.* **2005**, *24*, 87–98, (In Chinese with English abstract). [CrossRef]
78. Xiao, Y.; Feng, C.Y.; Li, D.X.; Liu, J.N. Chronology and fluid inclusions of the Guoluolongwa gold deposit in Qinghai province. *Acta Geol. Sin.* **2014**, *88*, 895–902, (In Chinese with English abstract).
79. Groves, D.I.; Santosh, M. The giant Jiaodong gold province: The key to a unified model for orogenic gold deposits? *Geosci. Front.* **2016**, *7*, 409–417. [CrossRef]

Disclaimer/Publisher's Note: The statements, opinions and data contained in all publications are solely those of the individual author(s) and contributor(s) and not of MDPI and/or the editor(s). MDPI and/or the editor(s) disclaim responsibility for any injury to people or property resulting from any ideas, methods, instructions or products referred to in the content.